TITLE

Uncovering an allosteric mode of action for a selective inhibitor of human Bloom syndrome protein

SHORT TITLE

An allosteric inhibitor of human BLM

AUTHORS

X. Chen[1], Y. Ali[2], C.E.L. Fisher[1], R. Arribas-Bosacoma[1], M.B. Rajasekaran[2], G. Williams[2], S. Walker[2], J.R. Booth[2], J.J.R. Hudson[2], S.M. Roe[3], L. H. Pearl[1], S. E. Ward[2,4*], F. M. G. Pearl[3*], A.W. Oliver[1*]

AFFILIATIONS

1. Cancer Research UK DNA Repair Enzymes Group, Genome Damage and Stability Centre, School of Life Sciences, University of Sussex, Falmer, BN1 9RQ, United Kingdom.
2. Sussex Drug Discovery Centre, School of Life Sciences, University of Sussex, Falmer, BN1 9QJ, United Kingdom.
3. School of Life Sciences, University of Sussex, Falmer, BN1 9QG, United Kingdom.
4. Medicines Discovery Institute, Park Place, Cardiff University, Cardiff, CF10 3AT, United Kingdom.

* wards10@cardiff.ac.uk, f.pearl@sussex.ac.uk or antony.oliver@sussex.ac.uk

ABSTRACT

BLM (Bloom syndrome protein) is a RECQ-family helicase involved in the dissolution of complex DNA structures and repair intermediates. Synthetic lethality analysis implicates BLM as a promising target in a range of cancers with defects in the DNA damage response, however selective small molecule inhibitors of defined mechanism are currently lacking. Here we identify and characterise a specific inhibitor of BLM's ATPase-coupled DNA helicase activity, by allosteric trapping of a DNA-bound translocation intermediate. Crystallographic structures of BLM-DNA-ADP-inhibitor complexes identify a hitherto unknown interdomain interface, whose opening and closing are integral to translocation of ssDNA, and which provides a highly selective pocket for drug discovery. Comparison with structures of other RECQ helicases provides a model for branch migration of Holliday junctions by BLM.

MAIN TEXT

INTRODUCTION

RECQ helicases catalyse the unwinding of duplex DNA with 3' to 5' directionality, driven by energy liberated by ATP-hydrolysis. As well as simple DNA duplexes, the various members of the RECQ helicase family (BLM, WRN, RECQ1, RECQ4 and RECQ5 in humans) are able to unwind DNA within a range of complex DNA structures and DNA repair intermediates, including: forks, bubbles, triple helices, displacement (D)-loops, G-quadraplexes, and 3 or 4-way Holliday junctions (extensively reviewed in[1,2]).

RECQ-helicases are strongly implicated in the maintenance of genomic integrity, principally through their participation in the homologous recombination (HR) pathway for repair of DNA double-strand breaks and restart of collapsed or blocked replication forks (reviewed in[1,3]), but also have roles in toleration of microsatellite instability[4,5] and sister chromatid decatenation[6]. Defects in RECQ-family members are responsible for rare genetic diseases displaying substantial genomic instability and cancer predisposition[7]. Loss of function of WRN underlies the complex progeria Werner Syndrome; defects in BLM underlie Bloom Syndrome, which is characterised by growth retardation and immunodeficiency; and defects in RECQ4 are associated with Rothmund-Thompson syndrome, which displays growth retardation, skeletal abnormalities and premature ageing.

A number of experimental and computational studies have implicated RECQ helicases – primarily BLM and WRN - as potential targets for cancer therapy, due to the synthetic lethality of their silencing or downregulation with genetic defects inherent in a range of different cancers [4,5,8-12]. Despite the therapeutic opportunities this presents, no drugs targeting RECQ helicases have yet been licensed, although potential leads have been reported[13-15].

Here we determine the mode of action for two reported inhibitors of BLM – ML216[13,14] and a substituted benzamide (compound **2**). While ML216 appears to act, at least in part, through direct DNA binding and has poor specificity, we find that **2** and derivatives thereof are highly specific binders of a defined BLM-DNA complex. Crystallographic analysis of the BLM-DNA-**2** complex identifies a novel allosteric binding site and reveals a distinctive conformational step in the helicase mechanism, that can be trapped by small-molecules. These data pave the way for the development of allosteric inhibitors of BLM helicase with the potential to generate trapped and highly cytotoxic BLM-DNA complexes.

RESULTS

Compound identification and screening

A series of compounds that targeted the helicase activity of human BLM were identified in a quantitative high-throughput screen (qHTS)[14], where the results were made publicly available from the PubChem data repository [https://pubchem.ncbi.nlm.nih.gov/bioassay/2528].

Filtering the 627 reported active compounds for preferential physicochemical properties (e.g. Lipinski's rule of five) and excluding those with potential pan-assay interference activity (PAINS) allowed us to group the compounds into several distinct clusters according to chemical similarity. The inhibitory activity of exemplars from each cluster were tested in a fluorescence-based DNA unwinding assay[14] against recombinant human BLM-HD (HD = helicase domain; amino acids 636-1298). However, only a single compound produced an IC_{50} lower than 10 μM (compound **1**, IC_{50} = 4.0 μM; **Fig.1A**).

We synthesised and purified 6 close analogues of this compound with the aim of generating preliminary structure-activity relationship data and confirmed their inhibitory activity in the unwinding assay (**Materials and Methods).** Compounds **2** to **6** inhibited the 3' → 5' helicase activity of recombinant human BLM-HD with IC_{50} values ranging from 2.2 to ~60 μM, whereas **7** did not inhibit BLM-HD over the concentration range tested (**Fig. 1A and S1, Table 1)**. An IC_{50} of 4 μM was determined for ML216, a compound reported to be a semi-selective inhibitor of human BLM[13,14], which was included as a positive control (**Fig. 1A)**.

In a malachite green-based assay that measures ATP turnover, we observed robust stimulation of hydrolysis by BLM-HD when the protein was incubated with a short single-stranded 20-base oligonucleotide (**Fig. 1B**). Here, we determined IC_{50} values ranging from 3.2 to ~50 μM for each of our active analogues and 4.4 μM for ML216 (**Fig. 1E and S1, Table 1**). Whilst the values of IC_{50} obtained in our orthogonal assay did not agree in absolute value with those determined in the first, it ranked each analogue with a similar order of potency.

Biophysical analysis of compound binding

We could readily observe changes in fluorescence, indicative of binding, upon titration of both ADP and ATP-γS into BLM-HD using microscale thermophoresis (MST, **Fig. S2A**). We could not however observe any interaction for our most potent compound **2**.

In the absence of biophysical evidence for binding, we sought to confirm that **2** wasn't just a false positive generated by interference with the fluorescent readout of the unwinding assay. An alternative gel-based assay allowed direct visualisation of the conversion of a forked DNA-

duplex into its component single-stranded oligonucleotides via the helicase activity of BLM-HD (**Fig. 2A**). Titration of **2** clearly inhibited production of the single-stranded DNA product in a dose-dependent manner, with a calculated IC_{50} of 1.8 μM (**Fig. 2B**).

Mode of Inhibition: DNA-interaction

Another potential false positive could be generated by compounds that bind directly to DNA, thus preventing BLM-HD from productively engaging with its substrate. To test this hypothesis, we used a commercial DNA-unwinding assay that utilises recombinant Topoisomerase I (Topo I) to relax a supercoiled plasmid. Compounds that intercalate or bind to the major or minor groove of the plasmid DNA prevent relaxation.

At the manufacturer's recommended concentration of 200 μM, the positive control m-Amsacrine (mAMSA) strongly inhibited relaxation of the supercoiled plasmid. In contrast, no effect was observed with **2** at the same concentration. However, partial inhibition of relaxation could be observed for a reaction containing ML216 (**Fig. 2C**). To confirm this observation, we purchased ML216 from an alternative commercial supplier (ML216-A) and also resynthesized and purified the compound in-house (ML216-B; **Materials and Methods**). In both cases, a similar level of inhibition was observed when the compounds were included in the relaxation assay, indicating that that this was both a real and reproducible effect (**Fig. 2C**).

To explore further the possibility that ML216 might interact directly with DNA, we tested its ability to displace SYBR Green II (SG2) from a DNA substrate in a dye displacement assay[16,17]. When SG2 binds to DNA, a concomitant increase in its fluorescence can be measured. If an added compound can compete with the dye for binding to the DNA, a corresponding decrease in the fluorescent signal is observed. We titrated ML216 into a forked-50mer dsDNA substrate, that had been pre-incubated with SG2, observing a clear time- and dose-dependent displacement of the dye, indicating that ML216 can directly interact with a DNA substrate (**Fig. 2D**).

Mode of Inhibition: ATP-competitive

With confidence that **2** was, in fact, a *bona fide* inhibitor of BLM, we repeated the unwinding assay in the presence a 10-fold higher concentration of ATP to examine if the compound was directly competitive with nucleotide binding to the active site of the enzyme. As the resulting IC_{50} value was identical to that previously determined, it ruled out this mode of inhibition, and suggested that the compound bound elsewhere **(Fig. S2B**).

Mode of Inhibition: Non-competitive

ATP-turnover experiments, under Michealis-Menten conditions, allowed us to generate a Lineweaver-Burk plot with data taken from DNA substrate titrations in the presence of 0, 5 and 10 μM of **2**. The resultant plot indicated a non-competitive (allosteric) mode of inhibition for **2** (**Fig. 2E**). With this information, we postulated that **2** might only bind to BLM-HD when it was engaged with a DNA substrate. We therefore revisited MST, first confirming the interaction of BLM-HD with single-stranded DNA oligonucleotides 15 and 20 bases in length (**Fig. 2F**). We next titrated **2** into the two pre-formed BLM-HD/ssDNA complexes. This time changes in fluorescent signal could be detected, confirming our hypothesis, with dissociation constants of 1.7 and 2.6 μM determined for the interaction with the 15mer and 20mer respectively (**Fig. 2G**).

Mode of Binding: *BLM-HD$^{\Delta WHD}$*

We created the expression construct BLM-HD$^{\Delta WHD}$ to remove the conformationally flexible Winged Helix domain (WH) that requires the presence of either a stabilising nanobody, or interaction with a large DNA substrate to facilitate crystallogenesis[18,19] replacing it with a short poly-(glycine/serine) linker that serves to connect the Zinc-binding domain (Zinc) directly to the Helicase and RNAse C-terminal domain (HRDC, **Fig. 3A**). In validation of this approach, we were able to crystallise the protein in complex with ADP and magnesium co-factor, and to determine its structure at a resolution of 1.53 Å; a significant increase in resolution over structures previously deposited in the PDB (4CDG, 2.8 Å; 4CGZ, 3.2 Å; 4O3M, 2.3 Å; see **Table S1**).

Superposition of the structures of BLM-HD (PDB: 4CDG) and BLM-HD$^{\Delta WHD}$ produces a rmsd of 0.86 Å over 2450 atom positions (D1 + D2 + Zn; PyMOL), indicating the overall conformation and geometry of the two recombinant proteins is highly similar, despite deletion of the WH domain (**Fig. S3A**). Furthermore, BLM-HD$^{\Delta WHD}$ binds both ssDNA-15mer and **2** with a similar affinity to that of BLM-HD (**Fig. S3B**).

Crystal structure of BLM-HD$^{\Delta WHD}$ in complex with compound 2 and ssDNA

We crystallised **2** in complex with BLM-HD$^{\Delta WHD}$, ADP/magnesium co-factor, and ssDNA-15mer (liganded complex); determining its structure at a resolution of 3.0 Å (**Table S1).** The complex crystallised in space group P1, with 6 molecules of BLM-HD$^{\Delta WHD}$ and associated ligands forming the asymmetric unit. Interestingly, the co-crystallised ssDNA-15mer helped drive formation of the crystal lattice, due to its partial self-complementary at the 5' end (5′-CGTAC-3′) that serves to form four consecutive base pairs between two oligonucleotides

(**Fig. 3B**); the cytosine at the 5' end of the oligonucleotide is not readily discernible in electron density maps and is therefore likely to be disordered. An extensive series of interactions are made to the bound nucleic acid by amino acids from all four sub-domains of the BLM-HD$^{\Delta WHD}$ expression construct (**Fig. S3C**).

Compound **2** sits in a small pocket found on the opposite face of the protein to that which binds nucleotide (**Fig. 3B, 3B inset)**, and integrates amino acid side chains from both the D1 and D2 subdomains of the helicase core, as well as several from the Zn-binding domain. The oxygen of the amino group at the centre of the compound is hydrogen-bonded to the side chain of Asn1022, whilst the nitrogen of the same moiety is in hydrogen-bonding distance to both the backbone oxygen and side chain of Ser801. The side chains of His805 and Thr1018 stack up against, and provide Van der Waals contacts to, the central ring system of the 3-amino-4,5-dimethylbenzenesulfonamide pendant group as part of a pocket lined by the side chains of residues Asp806, His1014, Thr1015, His1019 **(Fig.3C**). The nitrogen of the sulphonamide group is hydrogen-bonded to the side chain of Asp840, which itself is bonded to the side chain of His805. The 2-methyl-thiazole moiety of **2** sits against the surface of the alpha-helix containing Gly972 and is sandwiched by additional packing interactions with the side chains of Gln802 and Glu971. The side chains Thr832 and His798 also contribute to this section of the binding pocket, which is 'capped' by Gln975. The central benzene ring of **2** is also contacted by the side chains of Gln802 and Glu971.

Reconfiguration of the Aromatic-Rich Loop

The aromatic-rich loop (ARL) is a highly conserved motif in RecQ helicases that serves as a molecular 'sensor', detecting binding of single-stranded DNA and coupling it to structural rearrangements that enable ATP hydrolysis[20,21]. In our high-resolution structure of BLM-HD$^{\Delta WHD}$, the ARL is disordered and is not visible in electron-density maps (**Fig. 4A**). By contrast, it can be fully modelled in the liganded complex, but its conformation is distinct from that observed in PDB entries 4CDG and 4CGZ where the single-stranded extension of bound nucleic acid substrates does not extend across to the D1 domain (**Fig. 4B and S4A**).

Structures with a high degree of structural similarity to the liganded complex were identified with PDBeFold[22]. The search produced PDB entries 6CRM and 4TMU, with Q-scores of 0.47 and 0.46 respectively, which both describe structures of the catalytic core of *Cronobacter sakazakii* RecQ helicase (CsRecQ) in complex with different DNA substrates[20,23]. Comparison, in each case, reveals a close to identical conformation of the ARL to that observed in our liganded complex, as well as nucleic acid interactions that include the D1 domain (**Fig. S4B and C**).

For CsRecQ, Manthei *et al.* described concerted movements of residues Phe158 and Arg159, within the ARL to interact with the 3' single-stranded extension of their co-crystallised DNA substrate[20]; in our liganded complex the equivalent residues undergo a similar transition (Phe807 and Arg808 respectively). We observe that Phe158 moves to make base-stacking interactions with G8 and A9 of the bound ssDNA-15mer. By comparison to 4CDG, we also see that Arg808 switches from interacting with Asp806 of the ARL to the backbone oxygen of Pro715 and the side chain of Glu768 (**Fig. 4A and 4B**), Notably, mutation of residues equivalent to Arg808 or Glu768 in EcRecQ (Arg159 and Glu124) have been shown to perturb enzyme function[20,21]. Interestingly, in BLM, Asp806 is 'freed' to interact with the side chain of His1029, a residue within the Zn-binding domain (**Fig. 4B**).

In their 2017 paper, Newman *et al.*, proposed a general mechanism for the helicase activity of human RECQ5 (hsRECQ5) based on their analyses of the available crystal structures for RecQ-family helicases; indicating that 4TMU best represents a 'pre-ATP hydrolysis' conformational state[24]. In their structure of unliganded (apo) hsRECQ5 they report a polar contact between Gln345 and His160 of the ARL, which is subsequently broken as a result of binding to ATP, serving to free the ARL to interact productively with the single-stranded 3'-overhang of a bound DNA substrate. Importantly, they showed that mutation of glutamine 345 to alanine (Q345A) prevents stimulation of ATPase activity by binding to DNA, but does not perturb the basal rate of hydrolysis[24]. The importance of this particular residue is perhaps more apparent in *E. coli* RecQ, where mutation of the equivalent glutamine (Q322A) essentially ablates all ATPase capability[20]. Notably, in our liganded structure, the equivalent residues (Gln975 and His798 respectively) form part of the binding pocket for **2 (Fig. 3C, right and 4A)**.

HRDC from parked to DNA-engagement

The HRDC (Helicase and RNase D C-terminal domain) was originally identified as a putative nucleic-acid binding motif in both BLM and WRN (Werner syndrome helicase) and named in part for its similarity to a domain found at the C-terminus of *E. coli* RNase D[25]. However, only very weak ssDNA binding (K_d ~ 100 μM) has been reported for this domain in isolation[26].

In their paper describing the crystal structure of BLM in complex with DNA, Newman *et al*. observe that the HDRC domain packs against a shallow cleft formed between the D1 and D2 domains of the helicase core, with the interface between the different modules being highly polar in nature. Their follow-on small angle X-ray scattering experiments also indicate that the HRDC domain of BLM is free to disassociate and re-bind to the helicase core[18]. In our high-resolution crystal structure of BLM-HD$^{\Delta WHD}$ we observe the same 'parked' interaction for the

HRDC, even in the absence of the WHD (**Fig. S3A**), but in our liganded structure we see that the HRDC domain swings across the face of the core helicase fold (**Fig. 5A**) to make a series of polar interactions with the ssDNA-15mer, which is presented on the surface of the D1 domain of a second protomer within the asymmetric unit (**Fig. 3B and 5B**).

The side chains of HRDC residues Asn1242 and His1236, contained within the 'hydrophobic 3_{10} helix'[26], are hydrogen-bonded to the O4 group of the T12 base and the N3 of the G11 base, respectively. The side chain of Phe1238 is also involved in an edge to ring-stacking interaction with the G11 base. Each of these interactions is consistent with chemical shift changes previously observed in HSQC spectra - as a result of titrating ssDNA into ^{15}N-labelled BLM-HRDC[26] – suggesting that the observed interactions have biological relevance, and that our structure represents the first to capture HRDC interactions with ssDNA. Furthermore, amino acids residues Lys1227, Tyr1237, Thr1243, and Asn1239 are also in close proximity to the bound DNA (**Fig. 5B**) and could be expected to undergo changes in chemical environment upon interaction; again consistent with the reported perturbations in HSQC spectra[26]. Asn1239 might also be expected to pick up an additional contact with the 5'-phosphate of a subsequent nucleotide in an extended substrate.

Selectivity profile

With a robust molecular understanding for the binding mode for **2**, we next examined if the compound displayed selectivity for members of the RecQ-helicase family. In our ATP-turnover assay we saw no inhibition of recombinant helicase domains (HD) from human WRN, human RecQ5 or the unrelated *E. coli* helicase UvrD over the concentration range tested, whilst at higher concentrations inhibitory effects started to appear against human RecQ1. In contrast, ML216 robustly inhibited all four RecQ-family helicases tested and at higher concentrations also affected UvrD; in line with, and in support of, our observation that ML216 is non-specific and elicits at least part of its inhibitory effect by binding directly to DNA (**Fig. 6A**).

Whilst compound solubility prevented generation of a complete inhibition curve for UvrD and thus a robust estimate of IC_{50}, the estimated Hill coefficient (*n*H) was close to 1 — in contrast to those calculated for titrations of ML216 against the RecQ helicases, which were generally steeper (ranging from 1.8 to 4.3), again suggesting that instead of a forming a 1:1 protein to inhibitor complex, there is in fact, a more complex (possibly mixed) mode of binding for this compound to this class of enzymes.

Conformational trapping

As binding of **2** has no direct effect on the ability of BLM-HD$^{\Delta WHD}$ to bind either ssDNA or nucleotide, we hypothesised that it might act to 'lock' the helicase into a conformational state where DNA substrates remain bound but cannot be unwound. In support of this idea, we undertook MST assays with a labelled single-stranded oligonucleotide in the both the presence and absence of **2**. Here, we observed a clear concentration-dependent decrease in K_d in the FP experiment when **2** was added, consistent with a decrease in the off-rate for DNA-binding, supporting our hypothesis that the compound acts to 'trap' BLM in its interaction with ssDNA (**Fig. 6B**).

DISCUSSION

Allosteric binding site

Compound **2** binds to a small pocket — hereinafter referred to as the allosteric binding site (ABS) — which is generated transitorily as part of the set of conformational changes that BLM undergoes during its catalytic cycle; relative movements of the D1 and D2 domains with respect to each other, upon interaction with nucleotide and DNA substrates, have previously been described by Newman *et al*[24]. Only when the D1 domain of BLM interacts with single-stranded DNA is the ARL in the correct conformation to permit compound binding, as then the side chain of Trp803 is repositioned and no longer occludes / fills the ABS (**Fig. 4A, B**).

Gyimesi *et al*. determined that the rate-limiting step for the unwinding activity of BLM is a structural transition between two ADP-bound states, which they suggest leads directly to 'stepping' along the single-stranded region of bound DNA substrates. They describe a so-called 'open' state where ADP can freely dissociate from the enzyme, and a 'closed' state that interconverts slowly to the open state in order to release ADP[27]. They also note that conversion between these states is accelerated in the presence of ssDNA.

Taken as a whole, our experimental data would be consistent with the notion of **2** acting to 'trap' or stabilise the 'closed' state, preventing conversion to the 'open' state, ADP release and thus DNA unwinding. Furthermore, compounds bound stably to the ABS should also sterically prevent the ARL from reverting to its initial conformation / structurally disordered state found at the beginning of the catalytic cycle (**Fig. 4A, B**).

However, this is perhaps at odds with the description of PDB entry 4TMU (CsRecQ, **Fig. S4**), to which our liganded complex is the most similar, as an example of the pre-ATP hydrolysis step of the RecQ-family helicase catalytic cycle[24]. A possible explanation, still consistent with our demonstration of 'trapping', is that binding of **2** prevents the changes that normally result

as a consequence of ATP-hydrolysis and phosphate-release, keeping the enzyme in an apparent pre-hydrolysis conformation. More detailed kinetic analyses will be required to distinguish between these mode-of-action models.

Selectivity through Helical Hairpin interactions

Several different regions of BLM interact with **2** when it is bound to the ABS, including amino acids from helicase motifs I and III, plus a short region just upstream of motif IV[28,29] (pre-motif IV, **Fig. 7**). Unsurprisingly, the amino acid sequence identity of each region across the RecQ-family is extremely high, and do not therefore provide a facile explanation for the observed selectivity of **2** (**Fig. 6A**). In particular, two of the amino acid side chains involved in hydrogen bonds with **2** are absolutely conserved in identity (motif I, Ser801; motif III, Asp840, **Figure 3C and 7**). Likewise, amino acids within these motifs involved in hydrophobic contacts with **2** are also highly conserved in identity/chemical property. However, the third hydrogen bonding interaction (made by Asn1022 to **2**) and its position within the 'Helical Hairpin' of the Zn-binding domain provides some insight, as both the length and amino acid composition of this loop is highly divergent across the RecQ-family and absent from RecQ4 (**Fig. 7**). There is no obvious consensus for any of the residues, in equivalent positions to those in BLM, involved in compound interaction. This observation provides a plausible route, though the addition or alteration of chemical groups to the core scaffold of **2**, for generating potent and highly selective inhibitors for the individual members of the RecQ-family of helicases.

Speculative model for the involvement of the HRDC in unwinding DNA substrates

During model building and evaluation of our liganded structure, we found that the nucleic-acid interactions made by the different sub-domains of BLM-HD$^{\Delta WHD}$ explain how the HRDC might contribute to the ability of BLM to unwind different types of DNA substrate — incorporating information taken from our own structure, as well as that for the interaction of the WHD with dsDNA from PDB entry 4CGZ (**Fig. 7B**).

Simple superposition of the two structures results in a clash of the HRDC (in our structure) with the WHD, however this is readily resolved by a small horizontal translation of the HRDC (roughly equivalent to adding an additional nucleotide to the single-stranded portion of the bound DNA substrate). We also note that, in our liganded structure, the polarity of the single-stranded DNA interacting with the HRDC is opposite to that of our model but with the understanding that is actually dictated by the packing arrangement of the molecules that serve to generate the crystal lattice; on examination, each of the observed HRDC interactions is fully compatible with binding to ssDNA in either orientation.

342 However, using the trajectories for each of the bound DNA substrates as positional markers
343 allows generation of a model for unwinding of a simple DNA duplex. The double-stranded
344 portion of the substrate is held in place through the previously described set of interactions
345 with the WHD domain[18]. The β-hairpin of the WH serves to separate the DNA duplex, with
346 one strand 'actively' engaged with the D1/D2 domains of the helicase core and the Helical
347 Hairpin of the Zn-binding domain. The second 'inactive' strand passes along the opposite
348 face of the WH β-hairpin, to subsequently interact with the HRDC domain, potentially acting
349 to prevent reversion and re-annealing of the DNA duplex. The relatively poor binding affinity
350 of the HRDC for ssDNA is compatible with this model, as it would allow iterative release and
351 recapture of the 'inactive' strand as the DNA substrate is unwound.
352
353 A model for how BLM might unwind a Holliday Junction has previously been reported[30]; but
354 this treats the HRDC domain as a static object, leaving in it the 'parked' position and making
355 no interactions with nucleic acid. Data published subsequent to this paper has indicated that
356 the HDRC plays a more fundamental role, for example the charge-reversal mutation N1239D
357 to has been shown to ablate interaction of the HRDC with both ssDNA and a Holliday junction
358 substrate[26]. The HRDC has also been reported to confer DNA-structure specificity to BLM,
359 with Lys1270 playing a role in mediating interactions with DNA and for efficient dissolution of
360 double-Holliday junction substrates *in vitro* [31]. Consistent with this, our structural data reveals
361 that both Asn1239 and Lys1270 of the HDRC are poised to interact with a section of single-
362 stranded DNA just one to two nucleotides longer than that captured in our crystal lattice (**Fig.**
363 **5B**). Finally, our model also suggests the existence of a transient direct interaction between
364 the WHD and the HRDC.
365
366 Compound 2 itself, is unlikely to be suitable as a therapeutic agent, due to its poor ability to
367 penetrate the cell membrane of mammalian cells (data not shown). However, as the first
368 described *bona fide* selective allosteric inhibitor of human BLM, the understanding of its mode
369 of action will aid ongoing efforts to develop molecules targeting this class of enzymes for the
370 treatment of human disease.

MATERIALS AND METHODS

Compound synthesis and purification

Details for synthesis and purification of compounds is provided in supplementary information.

Expression constructs

Synthetic genes, codon-optimised for expression in *E. coli*, were purchased from GeneArt [ThermoFisher Scientific, Loughborough, UK]. With the exception of RECQ5 (see below) the coding sequence was subcloned into an in-house modified pET-17b vector at the NdeI and EcoRI sites of the multiple cloning site.

BLM-HD, BLM-HD$^{\Delta WHD}$: pAWO-STREP-3C; a pET-17b expression vector modified to encode an N-terminal human rhinovirus 3C-protease (HRV-3C) cleavable StrepII-affinity tag. BLM-HD encodes amino acids 636-1298 of human BLM (UniProt ID: BLM_HUMAN), whereas BLM-HD$^{\Delta WHD}$ encodes amino acids 636-1074 and 1231-1298.

RECQ1-HD: pAWO-His-TRX-3C*; a* pET-17b expression vector modified to encode an N-terminal His_6-tagged *E. coli* Thioredoxin HRV-3C cleavable affinity/solubility tag. RECQ1-HD encodes amino acids 49-616 of human RECQ1 (Uniprot ID: RECQ1_HUMAN).

WRN-HD: pAWO-His-SUMO-3C; a pET-17b expression vector modified to encode an N-terminal His_6-tagged *S. cerevisiae* Smt3 (SUMO) HRV-3C cleavable affinity/solubility tag. WRN-HD encodes amino acids 481-1521 of human WRN (Uniprot ID: WRN_HUMAN).

RECQ5-HD: The expression construct pNIC28-Bsa4-RecQL5 was obtained from the Structural Genomics Consortium, Oxford [see https://www.thesgc.org/tep/RECQL5 for full details]. RECQ5-HD encodes amino acids 11-526 of human RECQ5 (Uniprot ID: RECQ5_HUMAN).

Expression and purification

BLM-HD, BLM-HD$^{\Delta WHD}$

E. coli strain BL21(DE3) [Promega, Southampton, UK] was transformed with the required expression plasmid. A 'starter' culture was generated by inoculating a 250 ml glass Erlenmeyer flask with 100 ml of Turbo-broth [Molecular Dimensions, Sheffield, UK] supplemented with 50 μg/ml ampicillin. The culture was allowed to grow in an orbital-shaking incubator set at 37°C, 220 rpm, until the absorbance at 600 nm reached 1.5. The culture was then stored at 4°C until the following day. 12 ml of the 'starter' culture was used to inoculate

a 2 L Erlenmeyer containing 1 L of Turbo-broth supplemented with antibiotic as before. The culture was grown until the absorbance at 600 nm reached 1.5, when the flask containing the culture was placed on ice for a period of 30 minutes. During this time, the incubator temperature was reduced to 20°C. After incubation on ice, isopropyl-β-D-thiogalactoside (IPTG) was added to a final concentration of 0.4 mM, to induce protein expression. The flask was then returned to the incubator, and the culture allowed to grow overnight at the reduced temperature of 20°C. Cells were harvested by centrifugation after a period of 16 hours. The resultant cell pellet was stored at -20°C until required.

The cell pellet arising from 2 L of culture was resuspended, on ice, in 25 ml of Buffer A (50 mM HEPES-NaOH, pH 7.5, 1 M NaCl, 0.5 mM TCEP, 0.5 mM EDTA) supplemented with a protease inhibitor tablet [cOmplete EDTA-free Protease Inhibitor Cocktail Tablet; Roche, Burgess Hill, UK]. The cells were lysed by sonication and insoluble material removed by centrifugation. The resultant supernatant was applied to a 5ml Strep-Tactin Superflow Plus Cartridge [Qiagen, Manchester, UK], pre-equilibrated with Buffer A. Unbound material was application of 10 column volumes (CV) of Buffer A (50 ml). Retained proteins were then eluted from the column by application of 5 CV of Buffer B (Buffer A supplemented with 5 mM desthiobiotin). Fractions containing the required protein were identified by SDS-PAGE, pooled, and then concentrated to a final volume of 2.5 ml using centrifugal concentrators [Vivaspin 20, 5000 MWCO; Sartorius Stedim Biotech GmBH, Goettingen, Germany]. After overnight cleavage of the affinity tag with human rhinovirus 3C-protease, the sample was diluted to reduce the NaCl concentration to below 250 mM. This was applied to a 5 ml HiTrap Heparin HP cartridge [GE Healthcare Life Sciences, Little Chalfont, UK], pre-equilibrated in Buffer C [50 mM HEPES-NaOH, pH 7.5, 250 mM NaCl, 0.5 mM TCEP, 0.5 mM EDTA]. Unbound material was removed by washing the column with 10 CV of buffer C. A linear NaCl gradient starting at a concentration of 250 mM and ending at 2000 mM, over 50 CV, was applied to the column. Fractions containing the desired recombinant protein were identified, pooled and concentrated as before. The concentrated sample was then applied to an HiLoad 26/600 Superdex 200 size exclusion chromatography column [GE Healthcare] pre-equilibrated in Buffer D [20 mM HEPES-NaOH pH7.5, 250 mM NaCl, 0.5 mM TCEP]. Again, fractions containing the desired recombinant protein were identified, pooled and concentrated, then flash-frozen in aliquots in liquid nitrogen and stored at -80°C until required.

RecQ1-HD, RecQ5-HD, WRN-HD

Expression and purification of RecQ1-HD, RecQ5-HD and WRN-HD were achieved using procedures similar to that used for BLM-HD, but with initial capture achieved using an IMAC

column. Samples were applied to a HiTrap 5 ml TALON Crude column [GE Healthcare] pre-equilibrated in Buffer A [50 mM HEPES-NaOH pH 7.5, 500 mM NaCl, 0.5 mM TCEP, 10 mM imidazole]. The column was washed with 5 column volumes of Buffer A, with retained protein eluted by the addition of 5 CV of Buffer B (50 mM HEPES-NaOH pH 7.5, 500 mM NaCl, 0.5 mM TCEP, 300 mM imidazole). Affinity/solubility tags were removed by incubation with either HRV-3C (RecQ1, WRN) or TEV protease (RecQ5).

UvrD

Purified recombinant *E. coli* UvrD was kindly provided by Dr. Mohan Rajasekaran (Sussex Drug Discovery Centre, University of Sussex, UK).

REAGENTS

Solutions

Mg-ATP = 50 mM $MgCl_2$, 50 mM ATP

Mg-ADP = 50 mM $MgCl_2$, 50 mM ADP

Oligonucleotides

Reverse-phase purified oligonucleotides were purchased from either Kaneka Eurogentec S.A. (Seraing, Belgium) or Eurofins Genomics Germany GmbH (Ebersberg, Germany).

ssDNA-15mer: 5'-CGTACCCGATGTGTT-3'

ssDNA-20mer: 5′-CGTACCCGATGTGTTCGTTC-3′

Forked-50mer:

A: 5′-XGAACGAACACATCGGGTACGTTTTTTTTTTTTTTTTTTTTTTTTTTTTT-3′

B: 5′-TTTTTTTTTTTTTTTTTTTTTTTTTTTTTTTTCGTACCCGATGTGTTCGTTCY-3′

Where X and Y are the following modifications:

Unwinding assay; X = BHQ2 (Black Hole Quencher 2), Y = TAMRA (tetramethylrhodamine)

Gel-based assay; X = none; Y = TAMRA

Dye-displacement assay; X = none; Y = none

FORK-A and FORK-B were annealed at a concentration of 200 μM using a slow-cooling cycle programmed into a PCR thermal cycler, in a buffer containing 20 mM HEPES.NaOH pH 7.5, 50 mM NaCl and 1 mM $MgCl_2$.

Commercially sourced ML216

ML216 was purchased from Merck KGaA (Darmstadt, Germany), product code: SML0661. ML216-A was purchased from Cayman Chemical (Ann Arbor, Michigan USA), product code: 15186.

BIOCHEMICAL ASSAYS

Fluorescence-based DNA unwinding assay

Methodology is based on that previously reported by Rosenthal *et al*[14]. Briefly, assays were carried out in 384-well black plates, with measurements taken at emission and excitation wavelengths of 540 and 590 nm respectively, in a PHERAstar multimode plate reader [BMG Labtech]. Assay buffer: 50 mM Tris-HCl pH 8.0, 50 mM NaCl, 2 mM $MgCl_2$, 0.01% v/v Tween-20, 2.5 µg/ml poly(dI-dC), 1 mM DTT.

28 µl of BLM-HD (at 0.535 nM in assay buffer) was pre-incubated with 2 µl of compound (2 mM stock dissolved in 100% v/v DMSO, over a range of final concentrations up to 100 µM) for a period for 15 minutes at room temperature. Next, 10 µl of substrate (40 nM forked-50mer dsDNA and 2000 µM Mg-ATP) was added, then incubated for a further 20 minutes at room temperature, before the final fluorescent intensity for each well was measured.

Assay conditions (compounds **2** to **7** and ML216): 0.375 nM BLM-HD, 10 nM annealed DNA substrate, 500 µM Mg-ATP in a reaction volume of 40 µl over a 20-minute incubation period.

Data for compound **1** are taken from an earlier iteration of the assay and were measured used the conditions: 3.75 nM BLM-HD, 75 nM annealed DNA substrate, 120 µM Mg-ATP in a reaction volume of 40 µl over a 20-minute incubation period.

Malachite-Green ATP turnover assay

Assay uses the PiColorLock Gold Phosphate Detection System from Innova Bioscience following the manufacturer's recommended protocol. Briefly, assays were carried out in 96-well clear flat-bottomed plates, with absorbance measurements taken at a wavelength of 630 nm in a CLARIOstar multimode plate reader [BMG Labtech]. Assay buffer: 50 mM Tris-HCl pH 7.5, 50 mM NaCl, 2 mM $MgCl_2$, 0.05% v/v Tween-20, 0.5 mM TCEP.

165 µl of BLM-HD and ssDNA-20mer (at a concentration of 2.4 nM and 121 nM, respectively) was pre-incubated with 10 µl of compound (2 mM stock dissolved in 100 % v/v DMSO, over a range of final concentrations up to 100 µM) for a period of 15 minutes at room temperature. Next, 25 µl of Mg-ATP substrate (at 16 mM) was added. After 20 minutes, reactions were

stopped by the addition of 50 μl Gold mix (a 100:1 ratio of PiColorLock:Accelerator reagents). After 2 minutes, 20 μl of stabiliser solution was added to each well. After a further 30 minutes absorbance measurements were taken.

Assay conditions: 2 nM BLM-HD, 100 nM ssDNA-20mer and 2 mM Mg-ATP in a reaction volume of 200 µL over a 20-minute incubation period.

Gel-based assay

Assay buffer: 50 mM Tris-HCl pH 8.0, 50 mM NaCl, 2 mM $MgCl_2$, 0.01% v/v Tween-20, 2.5 µg/ml poly(dI-dC), 1 mM DTT. 28 μl of BLM-HD (at a concentration of 2.9 nM) was pre-incubated with 2 μl of compound (2 mM stock dissolved in 100 % v/v DMSO, over a range of concentrations up to 100 µM) for a period of 15 minutes at room temperature. Next, 10 µl of substrate (300 nM forked-50mer dsDNA and 4.8 mM Mg-ATP) were added. After 10 minutes, reactions were terminated by the addition of 1 x loading dye (6 x solution: 10 mM Tris-HCl pH 7.5, 0.03% w/v bromophenol blue, 60% v/v glycerol, 60 mM EDTA). The samples were then loaded onto a 15% native gel (29:1 acrylamide:bis-acrylamide, 0.5 x TBE), separated by electrophoresis, and then visualized using a FLA-1500 fluorimager [Fujifilm, Bedford, UK]. The intensity of each species on the gel was quantified using the analysis tools provided in the software package Fiji[32].

Topoisomerase I DNA-unwinding assay

Assay uses the DNA Unwinding Assay Kit from Inspiralis (Norwich, UK) following the manufacturer's recommended protocol. Resultant samples were applied to a 1% w/v agarose gel (in 1 x TAE buffer), separated by electrophoresis, stained with ethidium bromide, and then visualised with a UV-transilluminator / digital gel documentation system.

Dye-displacement assay

Fluorescence intensity was measured in a CLARIOstar multi-mode plate reader [BMG Labtech] with excitation and emission wavelengths of 485 nm and 520 nm respectively, in 384-well black plates. 28 µl of forked-50mer dsDNA (at a final concentration of 800 nM) was pre-incubated with 10 µl of SYBR Green II (1:200 dilution) for a period of 20 minutes at room temperature. 2 µl of compound (1 mM stock dissolved in 100 % v/v DMSO, over a range of final concentrations up to 50 µM) was then added. Measurements were taken after incubation times of 20, 45 and 60 minutes. Assay buffer: 50 mM Tris-HCl pH 8.0, 50 mM NaCl, 2 mM $MgCl_2$, 0.01% v/v Tween-20, 1 mM DTT.

Assay conditions: 800 nM annealed DNA substrate and 1:800 SYBR Green II in a reaction volume of 40 µL over a 20-minute incubation period.

BIOPHYSICAL ASSAYS

Microscale thermophoresis (MST)

Experiments were performed in a Monolith NT.115 instrument from NanoTemper Technologies GmbH (München, Germany). Purified recombinant protein was labelled using a Monolith NT RED-Maleimide Protein Labelling Kit supplied by the manufacturer, following the recommended protocol. 19 µl of BLM-HD (at a final concentration of 75 nM) was mixed with 1 µl of the required 'ligand' solution (ssDNA and / or compound) and incubated for 15 minutes at room temperature, before being transferred to 'premium' capillaries for measurement. Experiments were performed at a temperature of 25 °C, with settings of 20% excitation power, 20% MST power. Assay buffer: 50 mM Tris-HCl pH 7.5, 100 mM NaCl, 2 mM $MgCl_2$, 0.05% v/v Tween-20, 0.5 mM TCEP.

CRYSTALLOGRAPHY

BLM-HD$^{\Delta WHD}$ / ADP

Prior to setting up of crystallisation screens BLM-HD$^{\Delta WHD}$ at a concentration of 15 mg/ml was combined with glycerol (100% v/v) and Mg-ADP (50 mM) to produce final concentrations of 10% v/v and 2 mM respectively. 150 nl of the prepared complex was combined with 150 nl of crystallisation reagent in MRC2 sitting drop vapour diffusion experiments against a reservoir volume of 50 µl. Crystals were obtained in condition A8 of the Morpheus HT-96 screen (0.06 M divalents, 37.5% Buffer System 2 and 37.5% Precipitant Mix 4; Molecular Dimensions [Sheffield, UK] at 4°C after a period of approximately 1 week.

Divalents = 0.3M magnesium chloride, 0.3M calcium chloride
Buffer system 2 = 1M sodium HEPES, MOPS (acid) pH 7.5
75% Precipitant Mix 4 = 25% w/v MPD, 25% v/v PEG1000, 25% w/v PEG 3350

Cryoprotection for data collection was achieved by stepwise soaking of crystals in buffers containing increasing amounts of ethylene glycol, to a final concentration of 20% (v/v). Diffraction data to a resolution of 1.53 Angstrom were collected from a single crystal, on beamline I04 at the Diamond Light Source (Didcot, UK). Crystals were in space group $P2_1$ with one molecule of BLM-HD$^{\Delta WHD}$ plus associated ligands forming the asymmetric unit.

BLM-HD$^{\Delta WHD}$ / ADP / ssDNA-15mer / compound 2

BLM-HD$^{\Delta WHD}$ was mixed with ssDNA-15mer at a 1:1.2 molar ratio (protein:DNA) to produce a final concentration of 15 mg/ml with respect to protein. Compound **2** was then added to a final concentration of 3 mM (from a stock at 100 mM in 100% v/v DMSO) and incubated with the protein:DNA complex overnight at 4°C. Prior to setting up crystallisation trials the complex was combined with glycerol (100% v/v) and Mg-ADP (50mM) to produce final concentrations of 10% v/v and 2 mM respectively. 150 nl of the prepared complex was combined with 150 nl of crystallisation reagent in MRC2 sitting drop vapour diffusion experiments against a reservoir volume of 50 µl. Crystals were obtained in condition C9 of the Morpheus HT-96 screen (0.09 M NPS, 0.1M Buffer System, 30% Precipitant Mix 1, Molecular Dimensions) at 4°C after a period of approximately 1 week.

NPS = 0.3 M sodium nitrate, 0.3 M sodium phosphate dibasic, 0.3 M ammonium sulphate
Buffer System 1 = 1.0 M imidazole, MES monohydrate (acid) pH 6.5
60% Precipitant Mix 1 = 40% v/v PEG 500 MME, 20% w/v PEG 20000

Cryoprotection for data collection was achieved by stepwise soaking of crystals in buffers containing increasing amounts of ethylene glycol, to a final concentration of 20% (v/v). Diffraction data to a resolution of 3.0 Angstrom were collected from a single crystal, on beamline I03 at the Diamond Light Source (Didcot, UK). Crystals were in space group P1 with six molecules of BLM-HD$^{\Delta WHD}$ plus associated ligands forming the asymmetric unit.

Data processing and model building

Diffraction data were automatically processed at the synchrotron by the xia2 pipeline[33], using software packages DIALS[34,35] or XDS [36] and Aimless[37]. For BLM-HD$^{\Delta WHD}$/ADP, coordinates corresponding to the helicase domain were extracted from PDB entry 4O3M and provided as a search model for molecular replacement using Phaser[38]. For BLM-HD$^{\Delta WHD}$/ADP/ssDNA-15mer/compound 2, the rebuilt and refined coordinates for BLM-HD$^{\Delta WHD}$ were used as the search model. Initial models were extended and improved by iterative rounds of building in Coot[39] and refinement in either PHENIX[40] or BUSTER[41] to produce the final deposited models. Crystallisation and refinement statistics are provided in Supplementary Table 1.

Data plotting and analysis

All experimental data were plotted and analysed using GraphPad Prism[42].

REFERENCES

1. Croteau, D.L., Popuri, V., Opresko, P.L. & Bohr, V.A. Human RecQ helicases in DNA repair, recombination, and replication. *Annu Rev Biochem* **83**, 519-52 (2014).
2. Wu, Y. Unwinding and rewinding: double faces of helicase? *J Nucleic Acids* **2012**, 140601 (2012).
3. Urban, V., Dobrovolna, J. & Janscak, P. Distinct functions of human RecQ helicases during DNA replication. *Biophys Chem* **225**, 20-26 (2017).
4. Chan, E.M. et al. WRN helicase is a synthetic lethal target in microsatellite unstable cancers. *Nature* **568**, 551-556 (2019).
5. Lieb, S. et al. Werner syndrome helicase is a selective vulnerability of microsatellite instability-high tumor cells. *Elife* **8**(2019).
6. Chan, K.L., North, P.S. & Hickson, I.D. BLM is required for faithful chromosome segregation and its localization defines a class of ultrafine anaphase bridges. *EMBO J* **26**, 3397-409 (2007).
7. Bernstein, K.A., Gangloff, S. & Rothstein, R. The RecQ DNA helicases in DNA repair. *Annu Rev Genet* **44**, 393-417 (2010).
8. Pearl, L.H., Schierz, A.C., Ward, S.E., Al-Lazikani, B. & Pearl, F.M. Therapeutic opportunities within the DNA damage response. *Nat Rev Cancer* **15**, 166-80 (2015).
9. Aggarwal, M. & Brosh, R.M., Jr. Hitting the bull's eye: novel directed cancer therapy through helicase-targeted synthetic lethality. *J Cell Biochem* **106**, 758-63 (2009).
10. Wang, H. et al. BLM prevents instability of structure-forming DNA sequences at common fragile sites. *PLoS Genet* **14**, e1007816 (2018).
11. Behan, F.M. et al. Prioritization of cancer therapeutic targets using CRISPR-Cas9 screens. *Nature* **568**, 511-516 (2019).
12. Kategaya, L., Perumal, S.K., Hager, J.H. & Belmont, L.D. Werner Syndrome Helicase Is Required for the Survival of Cancer Cells with Microsatellite Instability. *iScience* **13**, 488-497 (2019).
13. Nguyen, G.H. et al. A small molecule inhibitor of the BLM helicase modulates chromosome stability in human cells. *Chem Biol* **20**, 55-62 (2013).
14. Rosenthal, A.S. et al. Discovery of ML216, a Small Molecule Inhibitor of Bloom (BLM) Helicase. in *Probe Reports from the NIH Molecular Libraries Program* (Bethesda (MD), 2010).
15. Yin, Q.K. et al. Discovery of Isaindigotone Derivatives as Novel Bloom's Syndrome Protein (BLM) Helicase Inhibitors That Disrupt the BLM/DNA Interactions and Regulate the Homologous Recombination Repair. *J Med Chem* **62**, 3147-3162 (2019).
16. Del Villar-Guerra, R., Gray, R.D., Trent, J.O. & Chaires, J.B. A rapid fluorescent indicator displacement assay and principal component/cluster data analysis for determination of ligand-nucleic acid structural selectivity. *Nucleic Acids Res* **46**, e41 (2018).
17. Tse, W.C. & Boger, D.L. A fluorescent intercalator displacement assay for establishing DNA binding selectivity and affinity. *Acc Chem Res* **37**, 61-9 (2004).

18. Newman, J.A. et al. Crystal structure of the Bloom's syndrome helicase indicates a role for the HRDC domain in conformational changes. *Nucleic Acids Res* **43**, 5221-35 (2015).
19. Swan, M.K. et al. Structure of human Bloom's syndrome helicase in complex with ADP and duplex DNA. *Acta Crystallogr D Biol Crystallogr* **70**, 1465-75 (2014).
20. Manthei, K.A., Hill, M.C., Burke, J.E., Butcher, S.E. & Keck, J.L. Structural mechanisms of DNA binding and unwinding in bacterial RecQ helicases. *Proc Natl Acad Sci U S A* **112**, 4292-7 (2015).
21. Zittel, M.C. & Keck, J.L. Coupling DNA-binding and ATP hydrolysis in Escherichia coli RecQ: role of a highly conserved aromatic-rich sequence. *Nucleic Acids Res* **33**, 6982-91 (2005).
22. Krissinel, E. & Henrick, K. Secondary-structure matching (SSM), a new tool for fast protein structure alignment in three dimensions. *Acta Crystallogr D Biol Crystallogr* **60**, 2256-68 (2004).
23. Voter, A.F., Qiu, Y., Tippana, R., Myong, S. & Keck, J.L. A guanine-flipping and sequestration mechanism for G-quadruplex unwinding by RecQ helicases. *Nat Commun* **9**, 4201 (2018).
24. Newman, J.A., Aitkenhead, H., Savitsky, P. & Gileadi, O. Insights into the RecQ helicase mechanism revealed by the structure of the helicase domain of human RECQL5. *Nucleic Acids Res* **45**, 4231-4243 (2017).
25. Morozov, V., Mushegian, A.R., Koonin, E.V. & Bork, P. A putative nucleic acid-binding domain in Bloom's and Werner's syndrome helicases. *Trends Biochem Sci* **22**, 417-8 (1997).
26. Kim, Y.M. & Choi, B.S. Structure and function of the regulatory HRDC domain from human Bloom syndrome protein. *Nucleic Acids Res* **38**, 7764-77 (2010).
27. Gyimesi, M., Sarlos, K. & Kovacs, M. Processive translocation mechanism of the human Bloom's syndrome helicase along single-stranded DNA. *Nucleic Acids Res* **38**, 4404-14 (2010).
28. Gorbalenya, A.E. & Koonin, E.V. Helicases - Amino-Acid-Sequence Comparisons and Structure-Function-Relationships. *Current Opinion in Structural Biology* **3**, 419-429 (1993).
29. Hall, M.C. & Matson, S.W. Helicase motifs: the engine that powers DNA unwinding. *Mol Microbiol* **34**, 867-77 (1999).
30. Kitano, K. Structural mechanisms of human RecQ helicases WRN and BLM. *Front Genet* **5**, 366 (2014).
31. Wu, L. et al. The HRDC domain of BLM is required for the dissolution of double Holliday junctions. *EMBO J* **24**, 2679-87 (2005).
32. Schindelin, J. et al. Fiji: an open-source platform for biological-image analysis. *Nat Methods* **9**, 676-82 (2012).
33. Winter, G., Lobley, C.M. & Prince, S.M. Decision making in xia2. *Acta Crystallogr D Biol Crystallogr* **69**, 1260-73 (2013).
34. Beilsten-Edmands, J. et al. Scaling diffraction data in the DIALS software package: algorithms and new approaches for multi-crystal scaling. *Acta Crystallogr D Struct Biol* **76**, 385-399 (2020).
35. Winter, G. et al. DIALS: implementation and evaluation of a new integration package. *Acta Crystallogr D Struct Biol* **74**, 85-97 (2018).
36. Kabsch, W. Xds. *Acta Crystallogr D Biol Crystallogr* **66**, 125-32 (2010).

37. Winn, M.D. et al. Overview of the CCP4 suite and current developments. *Acta Crystallogr D Biol Crystallogr* **67**, 235-42 (2011).
38. McCoy, A.J. et al. Phaser crystallographic software. *J Appl Crystallogr* **40**, 658-674 (2007).
39. Emsley, P. & Cowtan, K. Coot: model-building tools for molecular graphics. *Acta Crystallogr D Biol Crystallogr* **60**, 2126-32 (2004).
40. Liebschner, D. et al. Macromolecular structure determination using X-rays, neutrons and electrons: recent developments in Phenix. *Acta Crystallogr D Struct Biol* **75**, 861-877 (2019).
41. Bricogne, G. et al. BUSTER version 2.10.3. *Global Phasing Ltd., Cambridge, UK* (2020).
42. GraphPad Prism, v. *GraphPad Software Inc., La Jolla, CA, USA*.
43. Laskowski, R.A. & Swindells, M.B. LigPlot+: multiple ligand-protein interaction diagrams for drug discovery. *J Chem Inf Model* **51**, 2778-86 (2011).
44. Rosenthal, A.S. et al. Synthesis and SAR studies of 5-(pyridin-4-yl)-1,3,4-thiadiazol-2-amine derivatives as potent inhibitors of Bloom helicase. *Bioorg Med Chem Lett* **23**, 5660-6 (2013).
45. Schrödinger, L. The PyMOL Molecular Graphics System, Version 2.0.
46. PDBsum. https://www.ebi.ac.uk/thornton-srv/databases/pdbsum/Generate.html.

ACKNOWLEDGMENTS

General: We thank Will Pearce (Sussex Drug Discovery Centre) for discussions relating to assay development. We are also grateful to the Diamond Light Source Ltd., Didcot, UK for access to synchrotron radiation.

Funding: This work was supported by funding from: Chinese Scholarship Council (XC and FGMP), Wellcome Trust 110578/Z/15/Z (SEW), Cancer Research UK Programme Grant C302/A24386 (LHP and AWO).

Competing Interests: The authors declare no competing interests.

Author Contributions: Conceptualisation: SEW, LHP, FGMP, AWO; Methodology: GW, SW, JJRH, AWO; Investigation: XC, YA, CELF, RA-B, JRB, SMR, SEW, LHP, FGMP, AWO; Writing — Original Draft: AWO; Writing — Review and Editing: XC, LHP, AWO; Visualisation: AWO; Supervision: GW, SW, SEW, FGMP, AWO; Funding Acquisition: XC, FGMP, SEW, LHP, AWO.

Data and materials availability: Coordinates and structures factors have been deposited in the Protein Data Bank (PDB) with accession codes 7AUC and 7AUD.

Figure 1

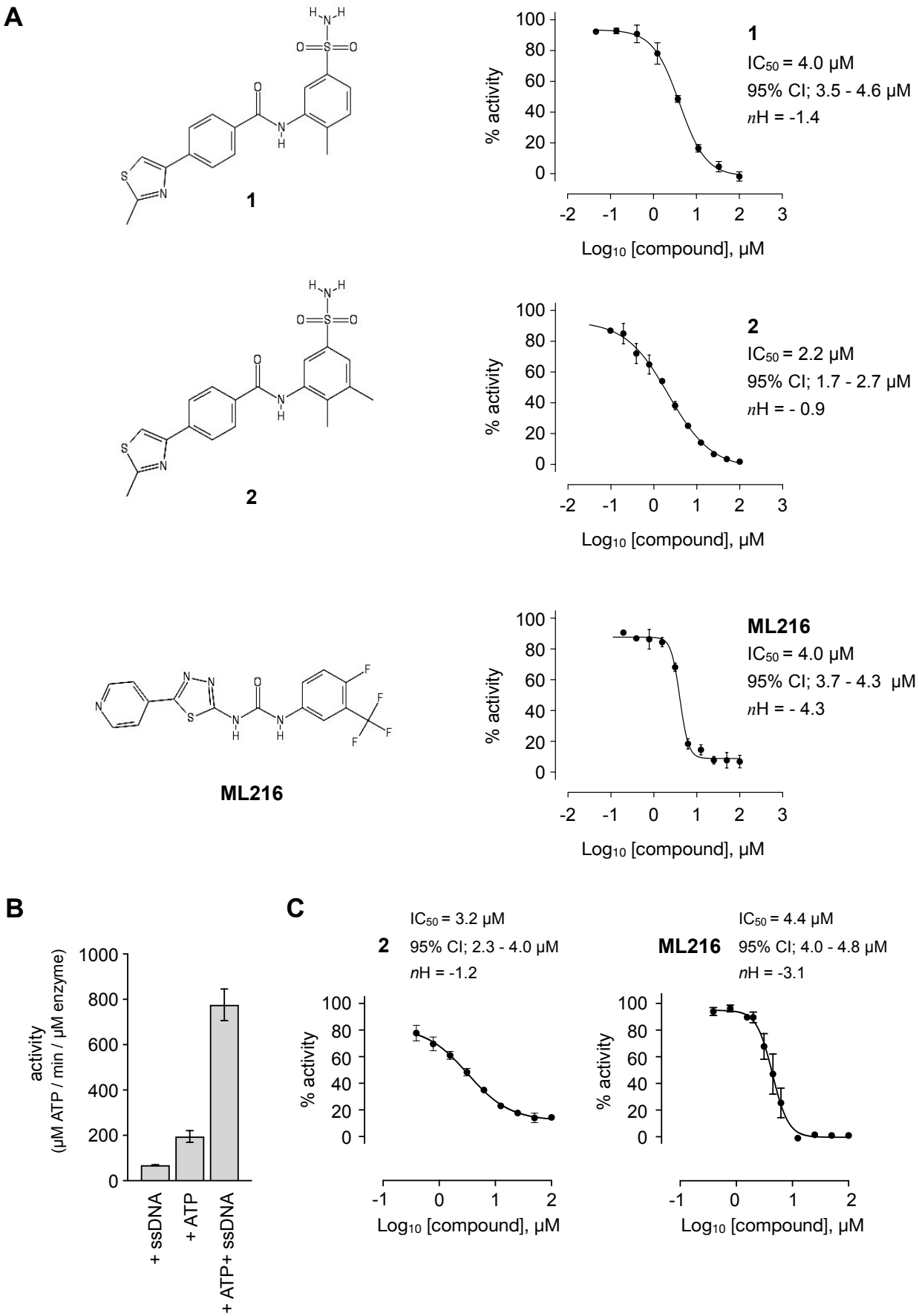

748 **Figure 1. Inhibition of BLM helicase unwinding activity**

749 (A, left) Chemical drawings for compounds **1**, **2** and ML216. (A, right) Dose response curves
750 from fluorescence-based DNA unwinding assays with BLM-HD. Experimental data were fitted
751 with a four parameter, log(inhibitor) vs. response model with variable slope. Calculated values
752 for IC_{50}, Hill slope (*n*H) and 95% confidence intervals (95% CI) are given in each case. (B)
753 Turnover of ATP by BLM-HD, as measured by a malachite-green end-point assay, is strongly
754 stimulated in the presence of a 20-base single-stranded oligonucleotide. (C) Dose response
755 curves from ATP-turnover assays with BLM-HD. Data were fitted as for (A). In each case data
756 points are the mean of 3 technical replicates, with error bars representing one standard
757 deviation (1 SD).

Figure 2

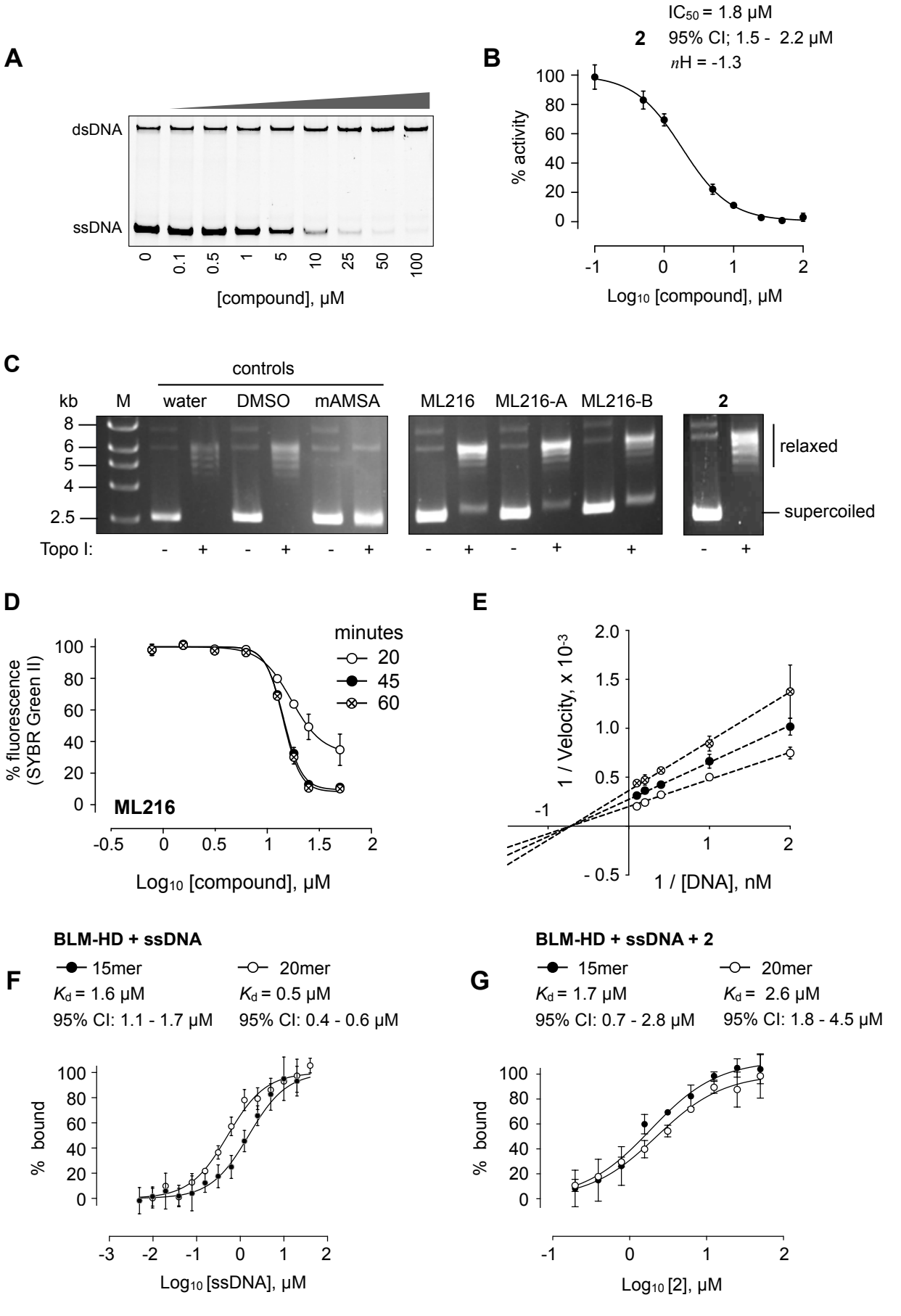

Figure 2. DNA interaction assays

(A) Titration of BLM-HD with **2** prevents the unwinding of a forked-50mer dsDNA substrate into its component strands, as judged by native gel electrophoresis**.** (B) Quantification of inhibitory activity by **2** in the gel-based activity assay. Experimental data were fitted with a four parameter, log(inhibitor) vs. response model with variable slope. Calculated values for IC_{50}, *n*H and 95% CI are given in each case. (C) Representative results from a Topoisomerase I (Topo I) DNA-unwinding assay. M = molecular mass maker; DMSO = buffer supplemented with dimethyl sulfoxide control; mAMSA = mAmsacrine; ML216, ML216-A, ML216B = refer to the three independent sources of the compound as described in the main text of the manuscript **(D)** Dose response curves from SYBR-Green II dye displacement assays, using a forked-50mer DNA duplex incubated with ML216 for a period of 20 (open circles), 45 (filled circles) and 60 minutes (crossed circles). Fitted lines are intended as visual aids only. **(E)** Lineweaver-Burk plot for data generated at three compound concentrations (0, 5 and 10 μM) in a colourimetric ATP turnover assay. Linear regression produces an intercept of all data on the X-axis indicating that **2** is a non-competitive inhibitor (i.e. same K_m, altered V_{max} parameter). (**F, G**) Binding isotherms for binding of BLM-HD to ssDNA-15mer and -20mer, or to compound **2** in the presence of either oligonucleotide, as determined by microscale thermophoresis (MST). Experimental data were fitted with a one-site, specific binding model. Values for K_d and 95% CI are given in each case. For all plots, data represent the mean of three technical replicates with error bars representing 1 SD.

Figure 3

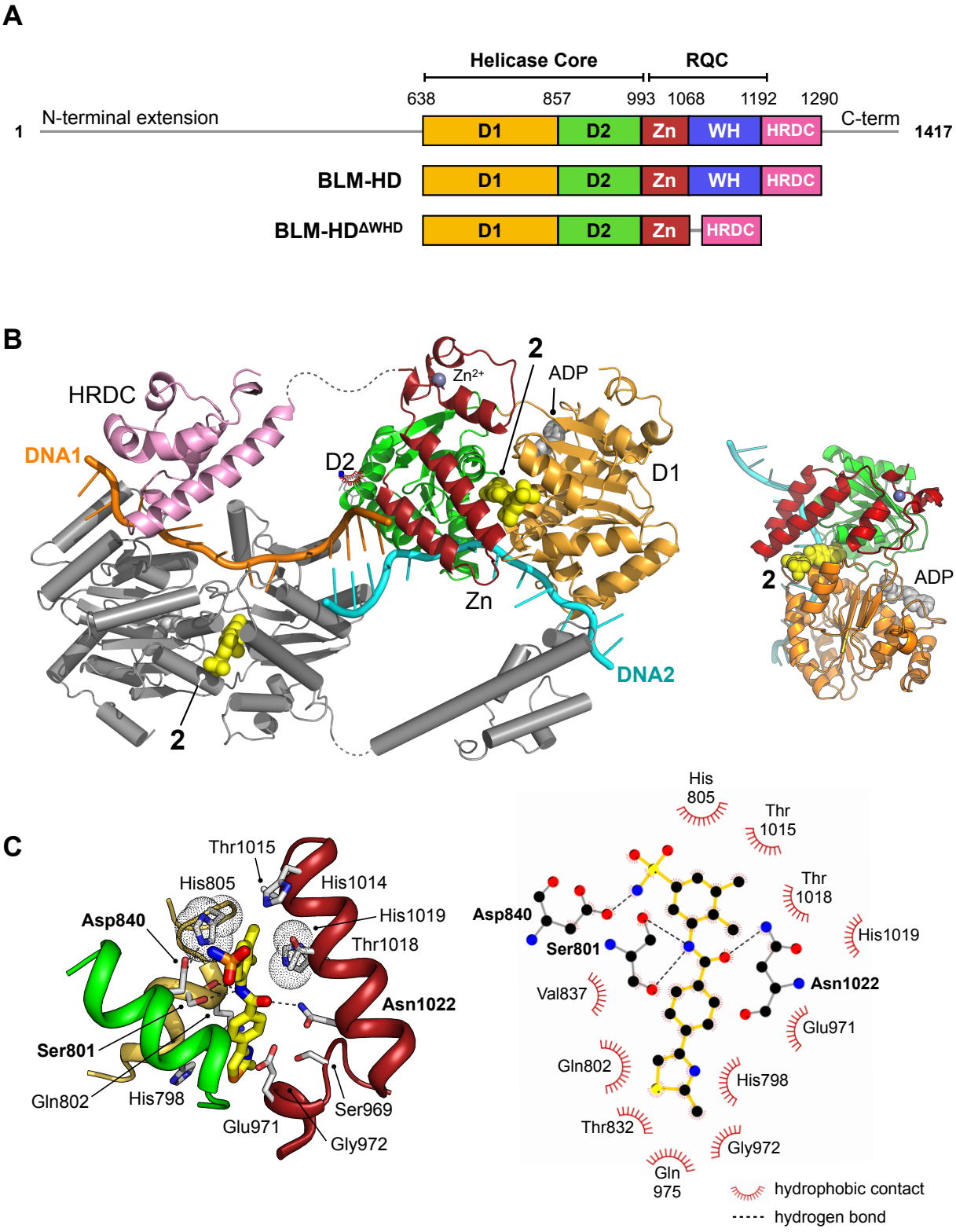

Figure 3. Structural overview of BLM-HD$^{\Delta WHD}$ in complex with compound 2

(A) Schematic representation of the domain composition and respective amino acid boundaries for full-length human BLM and the two expression constructs used in this study BLM-HD and BLM-HD$^{\Delta WHD}$. D1 and D2 = domains 1 and 2 of the helicase core; Zn = zinc-binding domain; WH = winged-helix; HRDC = Helicase and RNaseD C-terminal domain; RQC = RecQ C-terminal domain. (B and B inset) Molecular secondary structure cartoon highlighting components of a 'pseudo-symmetrical' dimer found in the asymmetric unit of BLM-HD$^{\Delta WHD}$ / Mg-ADP / **2** / ssDNA crystals**,** driven by partial complementarity of the single-stranded 15mer oligonucleotide at its 5' end (DNA1 and DNA2, coloured orange and cyan respectively). Compound **2** (yellow-coloured spheres) binds to a small pocket found on the opposite side to that which binds nucleotide (grey-coloured spheres). (C, left) Molecular cartoon representation highlighting interactions made between **2** and BLM-HD$^{\Delta WHD}$. Key amino acid residues are labelled and shown in stick representation, with carbon atoms coloured according to the schematic shown in panel A. Compound **2** is shown in stick representation, with carbon atoms coloured yellow. Potential hydrogen bonds are indicated by black dotted lines. (C, right) Modified LIGPLOT+[43] diagram of protein-compound interactions. See associated key for additional detail.

Figure 4

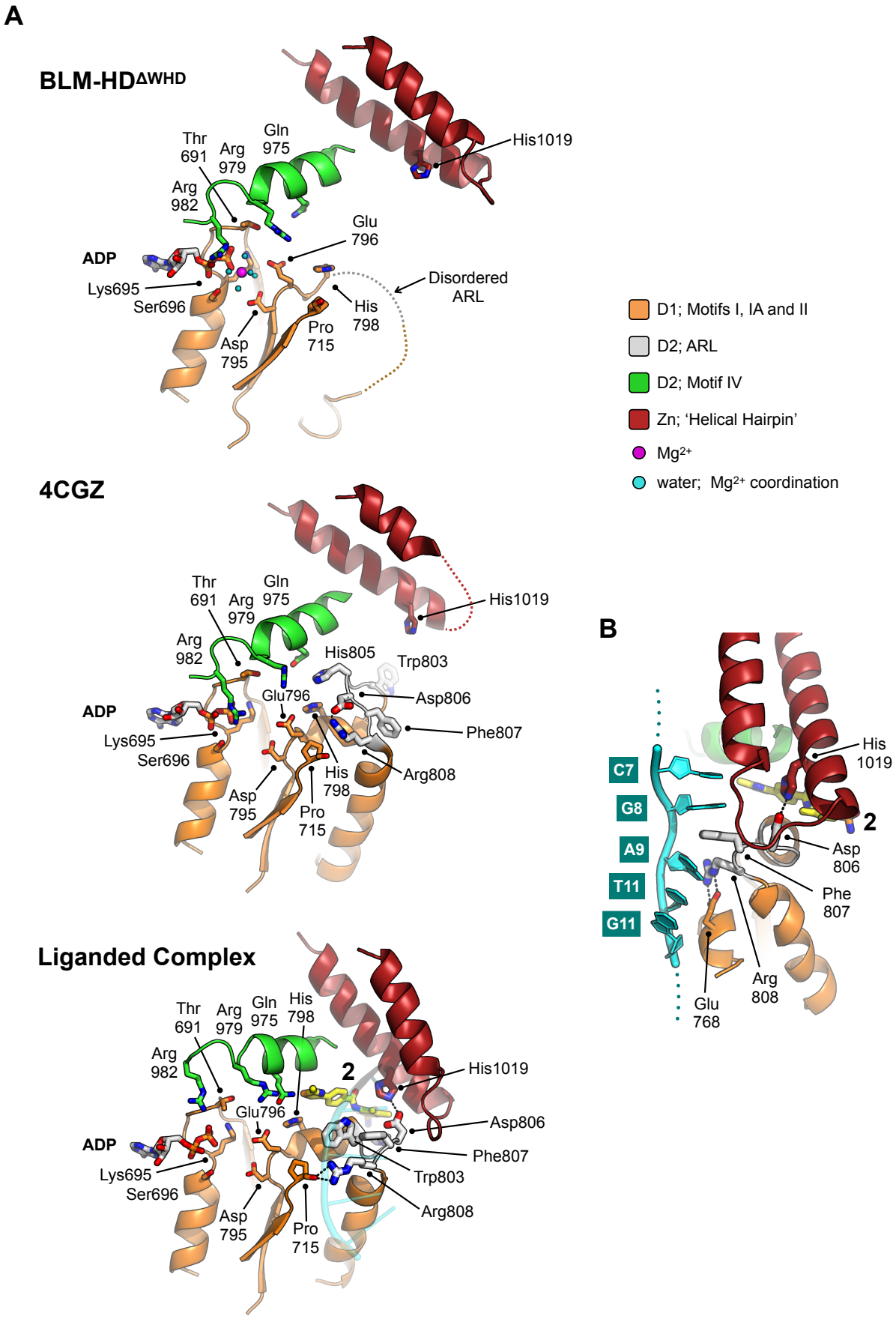

Figure 4. Structural transitions around the aromatic rich loop

(A) Molecular secondary structure cartoons for the region surrounding the aromatic rich loop (ARL) of BLM-HD$^{\Delta WHD}$ (top), PDB entry 4CGZ; BLM-HD in complex with DNA (middle) and liganded complex; BLM-HD$^{\Delta WHD}$ in complex with ADP, ssDNA-15mer and **2** (bottom). The side chains for key amino acid residues are shown in stick representation, with carbon atoms coloured according to their respective domains (see associated key). Bound ADP and **2** are also shown in stick representation, with carbon atoms coloured grey and yellow respectively. (B) Expanded and rotated view highlighting the interactions made between the ARL and ssDNA-15mer oligonucleotide (cartoon coloured cyan) in the liganded complex, also showing the relative position of compound **2**. Potential hydrogens bonds are represented by black dotted lines.

Figure 5

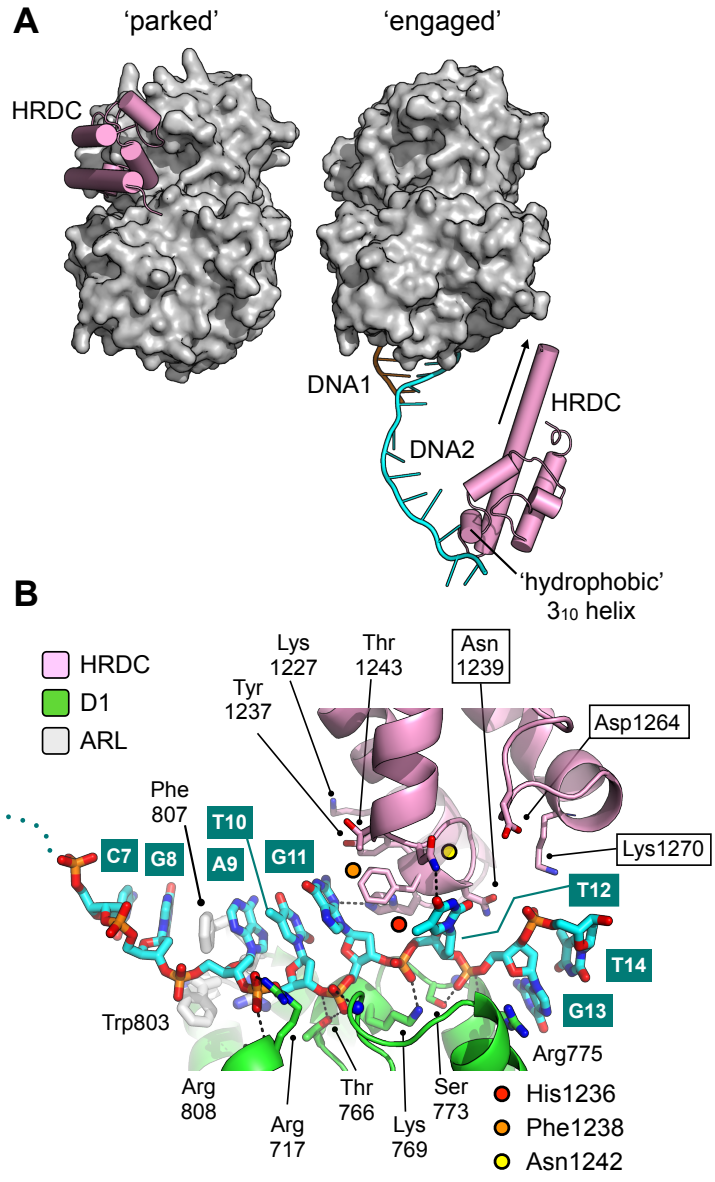

Figure 5. Repositioning of the HRDC domain

(A) Molecular surface representation of BLM-HD$^{\Delta WHD}$ (left) and the liganded complex (right) highlighting the relative positions of the HRDC domain (cylindrical helices coloured in pink). The HRDC moves from a 'parked' position located on one side of the helicase core, to an 'engaged' position on the other side in order to interact with the bound ssDNA-15mer. The N-terminus of the first HRDC alpha-helix is extended at the by ~ 6 aa, relative to the 'parked' position (as indicated by an arrow). (B) Molecular secondary structure cartoon highlighting interactions made by the HRDC to the bound ssDNA-15mer oligonucleotide. Side chains for key amino acid residues are shown in stick representation, with carbon atoms coloured according to their respective domains (see associated key). The bound ssDNA-15mer oligonucleotide is involved in interactions with both the D1 domain (carbon atoms coloured green) and the HRDC (carbon atoms coloured pink). Bound oligonucleotide is shown in stick representation, with carbon atoms coloured cyan.

Figure 6

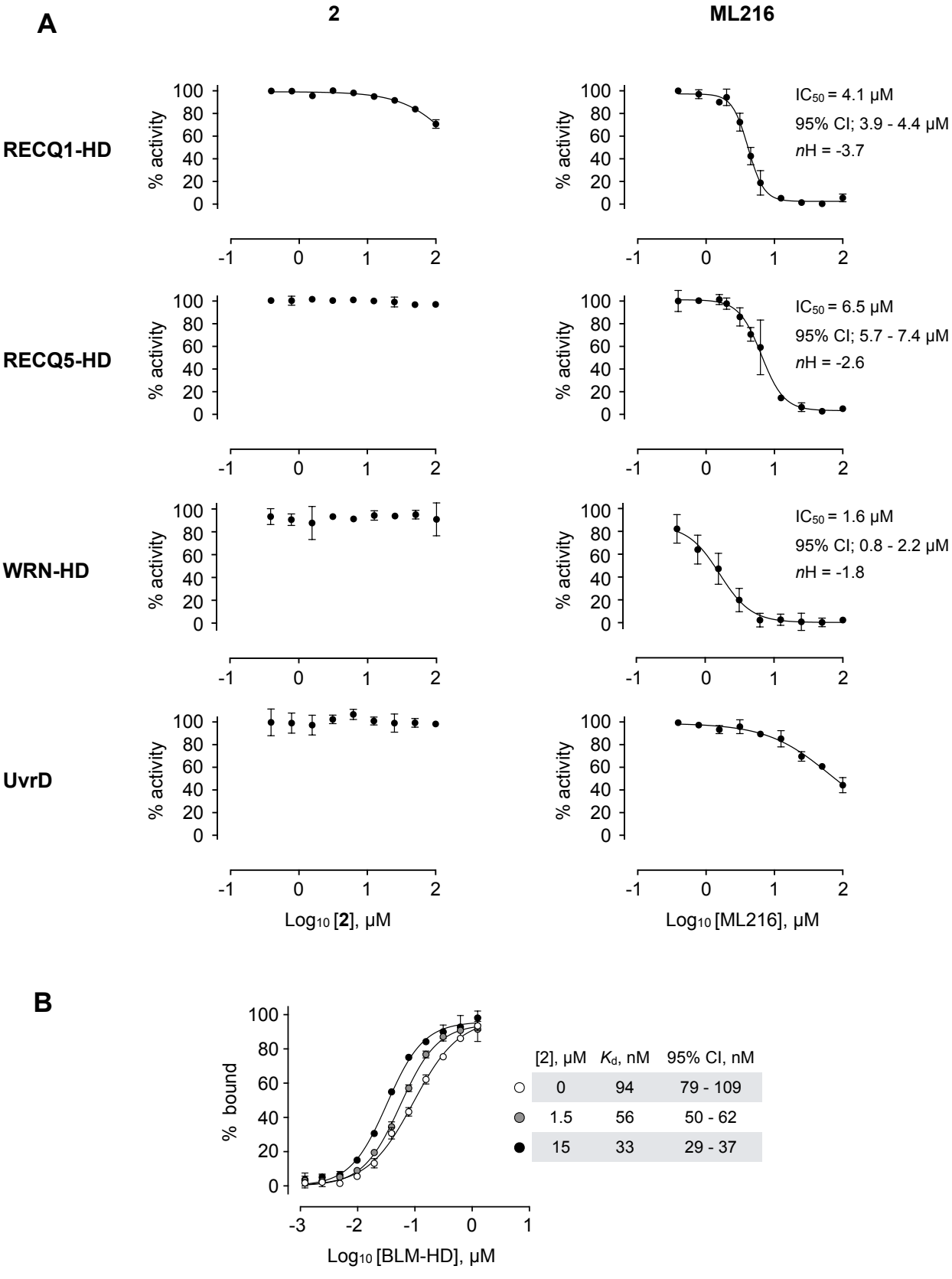

Figure 6. Selectivity profile of compound 2

(A) Dose response curves from ATP-turnover assays for titration of compounds **2** and ML216 against purified recombinant BLM-HD, WRN-HD, RecQ1-HD, RecQ5-HD and UvrD respectively. Calculated values for IC_{50}, *n*H and 95% CI are given in each case. **(B)** MST-derived binding isotherms for the interaction of BLM-HD with ssDNA-20mer in the presence of increasing concentrations of **2**. Calculated values for K_d and 95% CI are given in each case. For all plots, data represent the mean of three technical replicates with error bars representing 1 SD.

Figure 7

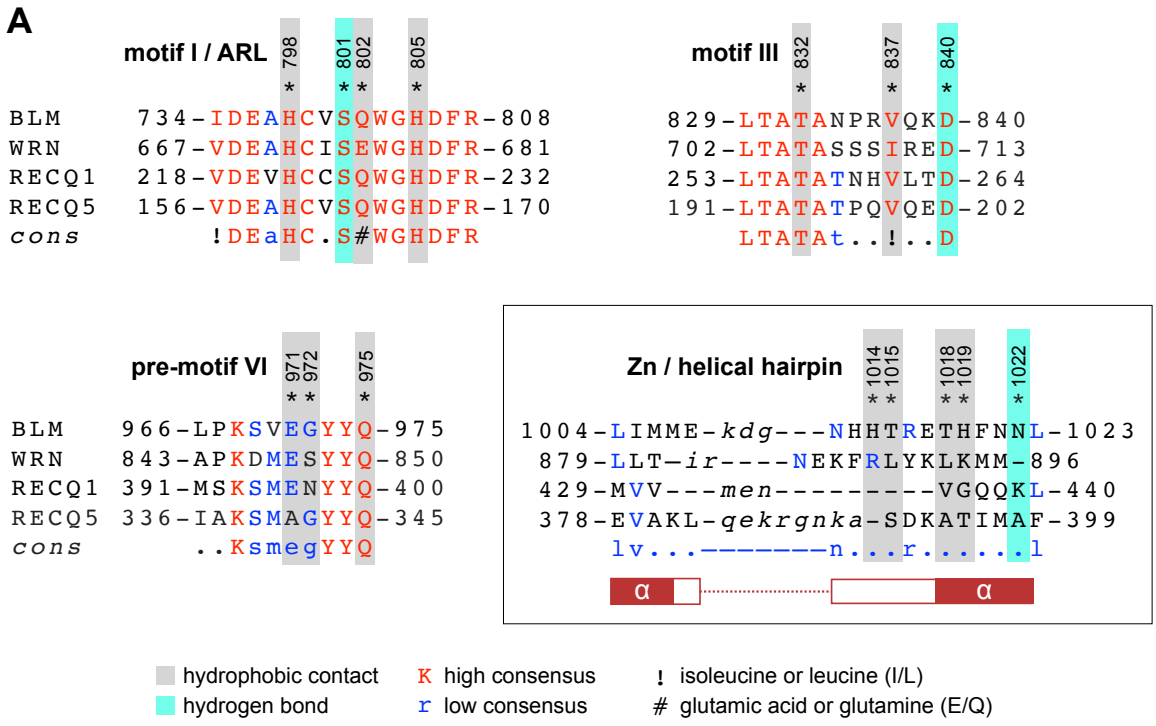

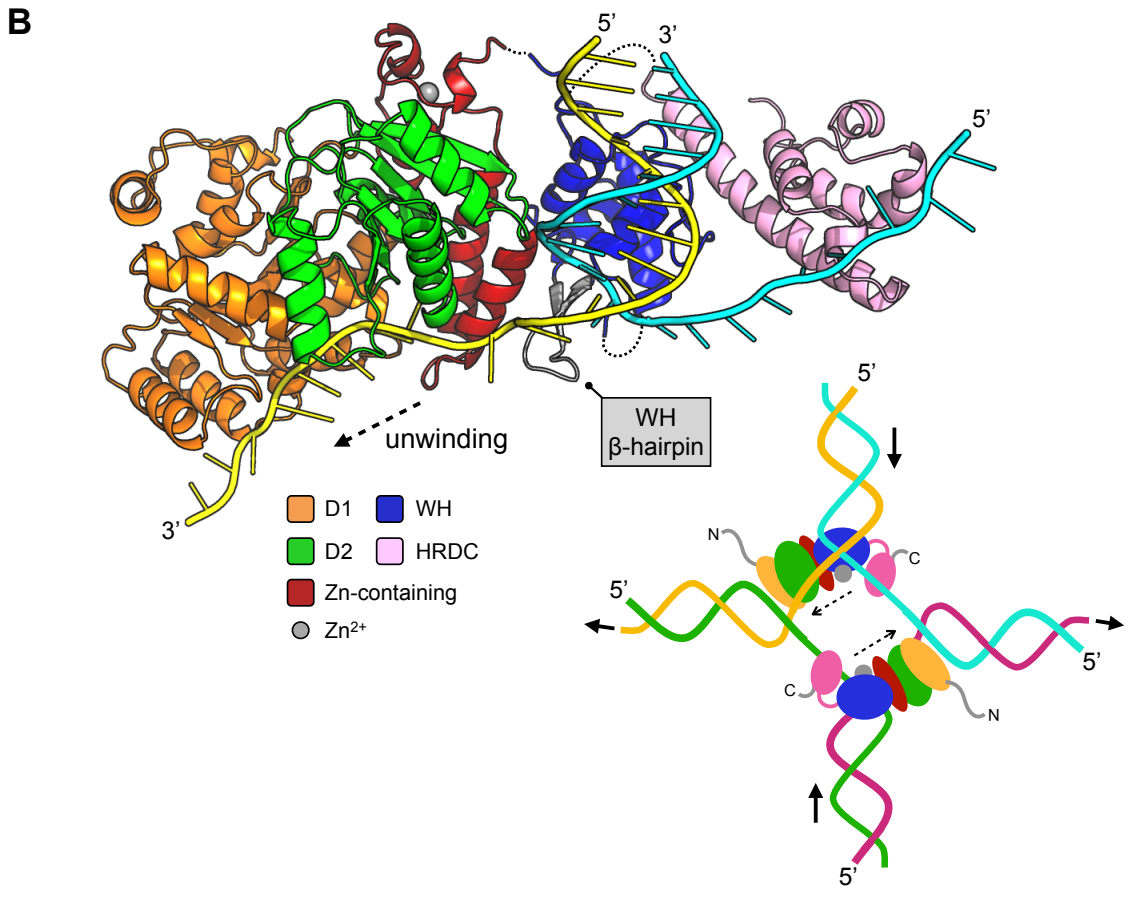

Figure 7. Compound selectivity / Speculative model

(A) The observed selectivity of compound **2** appears to arise from interactions made with amino acids of the Zn-binding domain 'Helical Hairpin' that are poorly conserved (or absent) from the other RecQ-family helicases. For each multiple amino acid sequence alignment shown, highly conserved amino acids are coloured in red. Those conserved in at least two RecQ family members (low consensus) are coloured blue. Amino acids residues of human BLM involved in interactions with **2** are additionally highlighted. Please see associated key for additional information. (B) A speculative model for how the HRDC domain may contribute to the unwinding of a DNA duplex or a Holliday junction (inset) via transient interactions with the passive or 'inactive' strand. See associated key for additional details.

		unwinding	turnover
#	Chemical Drawing	IC_{50} [95% CI]; μM	IC_{50} [95% CI]; μM
2	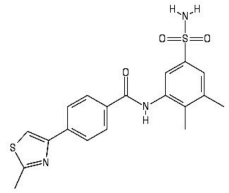	2.2 [1.7 – 2.7]	3.2 [2.3 – 4.0]
3	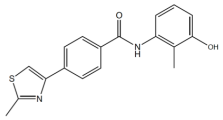	3.5 [2.4 – 5.2]	5.3 [4.7 – 6.1]
4	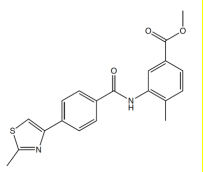	6.6 [3.4 – 12.7]	11.2 [8.3 – 15.3]
5	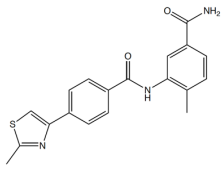	12.8 [4.5 – 36.8]	47.86 [18.28 – 180.7]
6	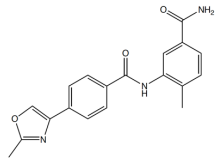	56.9 [25.4 – 171.3]	40.94 [15.9 – 139.8]
7	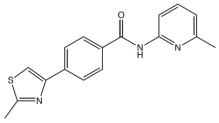	No inhibition	No inhibition
ML216	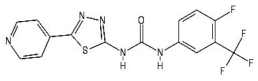	4.0 [3.7 – 4.3]	4.4 [4.0 – 4.8]

Table 1. Summary of inhibition data for seven exemplars from the identified compound series IC_{50} values were determined by fitting of experimental data to log (inhibitor) vs response models provided in GraphPad Prism. Data for the unwinding assay correspond to three technical replicates from a single experiment. For the ATP-turnover assay data correspond to at least two independent experiments, each containing three technical replicates.

SUPPLEMENTARY MATERIALS

Synthetic Preparation of Test Molecules

All reactions were conducted under an atmosphere of nitrogen unless otherwise stated. Anhydrous solvents were used as purchased or were purified under nitrogen as follows using activated molecular sieves. Thin layer chromatography was performed on glass plates pre-coated with Merck silica gel 60 F254. Visualisation was achieved with U.V. fluorescence (254 nm) or by staining with a phosphomolybdic acid dip or a potassium permanganate dip. Flash column chromatography was carried out using pre-packed columns filled with Aldrich silica gel (40-63 μm) on an ISCO Combiflash Rf, or a Biotage Isolera Prime. Proton nuclear magnetic resonance spectra were recorded at 500 MHz on a Varian 500 spectrometer (at 30 °C), using residual isotopic solvent ($CHCl_3$, δH = 7.27 ppm, DMSO δH = 2.50 ppm, 3.33 ppm (H_2O)) as an internal reference. Chemical shifts are quoted in parts per million (ppm). Coupling constants (J) are recorded in Hertz (Hz). Carbon nuclear magnetic resonance spectra were recorded at 125 MHz on a Varian 500 spectrometer and are proton decoupled, using residual isotopic solvent ($CHCl_3$, δC = 77.00 ppm, DMSO δC = 39.52 ppm) as an internal reference. Carbon spectra assignments are supported by HSQC and DEPT editing and chemical shifts (δC) are quoted in ppm. Infrared spectra were recorded on a Perkin Elmer FT-IR One spectrometer as either an evaporated film or liquid film on sodium chloride plates. Absorption maxima are reported in wave numbers (cm^{-1}). Only significant absorptions are presented in the data, with key stretches identified in brackets. LCMS data was recorded on a Waters 2695 HPLC using a Waters 2487 UV detector and a Thermo LCQ ESI-MS. Samples were eluted through a Phenomenex Lunar 3μ C18 50 mm × 4.6 mm column, using acetonitrile and water acidified by 0.01% formic acid in three methods: method 1 (3:7 to 7:3 acetonitrile and water over 7 minutes), method 2 (3:7 to 7:3 acetonitrile and water over 4 minutes) and method 3 (19:1 to 1:19 acetonitrile and water over 10 minutes), High resolution mass spectrometry (HRMS) spectra were recorded on Bruker Daltonics Apex III ESI-MS, with an Apollo ESI probe using a methanol spray. Only molecular ions, fractions from molecular ions and other major peaks are reported as mass/charge (m/z) ratios.

***N*-(2-methyl-5-sulfamoyl-phenyl)-4-(2-methylthiazol-4-yl)benzamide (1)**

Methyl 4-(2-bromoacetyl)benzoate

A solution of methyl 4-acetylbenzoate (1.00 g, 5.61 mmol) and *p*-toluenesulfonic acid monohydrate (54 mg, 0.28 mmol) in acetonitrile (30 mL) was treated with *N*-bromosuccinimide (0.99 g, 5.61 mmol) and the reaction mixture heated to 80 °C for 16 h. The solvent was removed under reduced pressure. The crude product was taken up in saturated aq. $NaHCO_3$ (15 mL) and extracted with ethyl acetate (3 × 15 mL). The combined organic components were then washed with brine (15 mL), dried over $MgSO_4$, filtered and concentrated under reduced

pressure. The crude product was purified by column chromatography (silica 24 g, 0 to 10% ethyl acetate in petroleum ether) to yield the desired compound as a light yellow solid (1.12 g, 70%). Rf 0.66 (petroleum ether:ethyl acetate, 9:1); ^{1}H-NMR (500 MHz, DMSO-d6) δ 8.14 – 8.01 (m, 4H, H-2, H-3), 4.98 (s, 2H, $COCH_2Br$), 3.89 (s, 3H, $COOCH_3$).

Methyl 4-(2-methylthiazol-4-yl)benzoate

To methyl 4-(2-bromoacetyl)benzoate (2.12 g, 8.23 mmol) in *N,N*-dimethylformamide (30 mL) was added thioacetamide (931 mg, 12.4 mmol) and the reaction mixture stirred at ambient temperature for 16 h. Upon completion, water was added to the reaction mixture. The resulting precipitate was collected by vacuum filtration and dried under reduced pressure to afford the desired compound as a white solid (1.48 g, 73%). m.p. 223–225 °C; ^{1}H-NMR (500 MHz, DMSO-d6) δ 8.14 (s, 1H, H-6), 8.08 (d, J 8.2, 2H, H-2), 8.01 (d, J 8.2, 2H, H-3), 3.87 (s, OCH_3), 2.73 (s, CH_3); ^{13}C-NMR (126 MHz, DMSO-d6) δ 166.5 (CO), 166.4 (C-8), 153.0 (C-5), 138.9 (C-4), 130.2 (C-2), 129.1 (C-1), 126.5 (C-3), 116.8 (C-6), 52.5 (OCH_3), 19.4 (CH_3); IR (neat, v_{max}, cm^{-1}) 3106, 2943, 1713, 1606, 1436, 1409, 1270, 1170; LCMS (LCQ) Rt = 2.9 min (method 2), m/z (ESI+) 234.2 $[M+H]^+$; HRMS m/z (ESI): calcd. for $C_{12}H_{11}NO_2S$ $[M+H]^+$ 234.0583, found 234.0583.

4-(2-Methylthiazol-4-yl)benzoic acid

To methyl 4-(2-methylthiazol-4-yl)benzoate (1.46 g, 6.26 mmol) in methanol (24 mL) and water (8 mL) was added sodium hydroxide (502 mg, 12.5 mmol) and the reaction mixture stirred at an ambient temperature for 16 h. Upon completion, the reaction mixture was acidified to pH of 2-3 using 2 M aq. hydrochloric acid solution. The resulting precipitate was collected by vacuum filtration and dried under reduced pressure to afford the desired acid as a white solid (1.21 g, 84%). m.p. 250–252 °C; ^{1}H-NMR (500 MHz, DMSO-d6) δ 8.10 (s, 1H, H-6), 8.05 (d, J 8.2, 2H, H-3), 7.99 (d, J 8.1, 2H, H-2), 2.73 (s, 3H, CH_3); ^{13}C-NMR (126 MHz, DMSO-d6) δ 167.5 (CO), 166.4 (C-8), 153.2 (C-5), 138.5 (c-4), 130.3 (C-2), 126.4 (C-3) , 116.5 (C-6), 19.4 (12-CH3). Quaternary 5-C not visible; IR (neat, v_{max}, cm^{-1}) 2826, 1667, 1608, 1573, 1421, 1290, 1169; 256 LCMS (LCQ) Rt = 0.6 min (method 1), m/z (ESI+) 220.2 $[M+H]^+$; HRMS m/z (ESI): calcd. for $C_{11}H_9NO_2S$ $[M+H]^+$ 220.0427, found 220.0428.

*N-(2-methyl-5-sulfamoyl-phenyl)-4-(2-methylthiazol-4-yl)benzamide (**1**)*

To 4-(2-methylthiazol-4-yl)benzoic acid (120 mg, 0.55 mmol), HBTU [(2-(1H-benzotriazol-1-yl)-1,1,3,3-tetramethyluronium hexafluorophosphate] (153 mg, 0.66 mmol), *N,N*-diisopropylethylamine (191 µL, 1.09 mmol) in *N,N*-dimethylformamide (2 mL) was added 3-amino-4-methylbenzenesulfonamide (102 mg, 0.55 mmol). The reaction mixture was stirred at ambient temperature for 16 h. Upon completion, the solvent was removed under reduced pressure. The crude product was taken up in ethyl acetate (5 mL), washed with saturated aq. $NaHCO_3$ (4 mL), brine (4 mL), dried over $MgSO_4$, filtered and concentrated under reduced pressure. The crude was purified by column chromatography (silica 12 g, 0 to 55% ethyl

acetate in petroleum ether) and further purified by column chromatography (amino silica 4 g, 0 to 5% methanol in dichloromethane) to yield the desired amide **1** as a white solid (15 mg, 7%). Rf 0.14 (petroleum ether:ethyl acetate 9:11); m.p. 261–263 °C; ^{1}H-NMR (500 MHz, DMSO-d6) δ 10.11 (s, 1H, CONH), 8.15 – 8.09 (m, 3H, H-3, H-6), 8.06 (d, J 8.2, 2H, H-2), 7.87 (s, 1H, H-6'), 7.62 (d, J 8.0, 1H, H-4'), 7.48 (d, J 8.0, 1H, H9'), 7.34 (s, 2H, SO_2NH_2), 2.75 (s, 3H, 8-CH_3), 2.32 (s, 3H, 2'-CH_3); ^{13}C-NMR (126 MHz, DMSO-d6) δ 166.4 (CO), 165.5 (C-8), 153.3 (C-5), 142.5 (C-5'), 138.3 (C-1), 137.6 (C-2'), 137.2 (C-2'), 133.6 (C-4), 131.2 (C-3'), 128.75 (C-2), 126.3 (C3), 124.1 (C-6'), 123.4 (C-4'), 116.1 (C-6), 19.4 (8-CH3), 18.44 (2'-CH3); IR (neat, v_{max}, cm^{-1}) 3258, 2923, 1630, 1572, 255 1516, 1444, 1403, 1304, 1154; LCMS (LCQ) Rt = 2.7 min (method 1), m/z (ESI+) 388.1 $[M+H]^+$; HRMS m/z (ESI): calcd. for $C_{18}H_{17}N_3O_3S_2$ $[M+H]^+$ 388.6847, found 388.6850.

***N*-(2,3-dimethyl-5-sulfamoyl-phenyl)-4-(2-methylthiazol-4-yl)benzamide (2)**

To 4-(2-methylthiazol-4-yl)benzoic acid (120 mg, 0.55 mmol), HBTU (153 mg, 0.66 mmol), *N,N*-diisopropylethylamine (0.19 mL, 1.09 mmol) in *N,N*-dimethylformamide (3 mL) was added), 3-amino-4,5-dimethylbenzenesulfonamide (110 mg, 0.55 mmol). The reaction mixture was stirred at ambient temperature for 16 h. Upon completion, the solvent was removed under reduced pressure. The crude product was taken up in ethyl acetate (5 mL), washed with saturated aq. $NaHCO_3$ (4 mL), brine (4 mL), dried over $MgSO_4$, filtered and concentrated under reduced pressure. The crude was purified by column chromatography (silica 12 g, 0 to 60% ethyl acetate in petroleum ether) to yield the desired amide **2** as a white solid (15 mg, 7%). Rf 0.12 (petroleum ether:ethyl acetate 1:1); m.p. 246–248 °C; ^{1}H-NMR (500 MHz, DMSO-d6) δ 10.17 (s, 1H, CONH), 8.13 – 8.08 (m, 3H, H-3, H-6), 8.05 (d, J 8.4, 2H, H-2), 7.64 (d, J 1.9, 1H, H-4'), 7.54 (d, J 1.9, 1H, H-3'), 7.28 (s, 2H, SO_2NH_2), 2.74 (s, 3H, 8-CH_3), 2.36 (s, 3H, 3'-CH_3), 2.17 (s, 3H, 2'-CH_3); ^{13}C-NMR (126 MHz, DMSO-d6) δ 166.4 (CO), 165.7 (C-8), 153.3 (C-5), 141.6 (C-5'), 138.5 (C-1), 137.6 (ArC), 137.5 (ArC), 137.1 (ArC), 133.7 (C-4), 128.7 (C-2), 126.3 (C-3), 124.6 (C-6'), 122.3 (C-4'), 116.1 (C-6), 20.7 (3'-CH3), 19.4 (8-CH3), 15.0 (2'-CH3); IR (neat, v_{max}, cm^{-1}) 3258, 2923, 1630, 1572, 1516, 1444, 1403, 1304, 1154; LCMS (LCQ) Rt = 2.0 min (method 1), m/z (ESI+) 402.1 $[M+H]^+$; HRMS m/z (ESI): calcd. for $C_{19}H_{19}N_3O_3S_2$ $[M+H]^+$ 401.0868, found 401.0866

***N*-(3-hydroxy-2-methyl-phenyl)-4-(2-methylthiazol-4-yl)benzamide (3)**

To 4-(2-methylthiazol-4-yl)benzoic acid (80 mg, 0.36 mmol) in dichloromethane (3 mL) was added oxalyl chloride (37 µL, 0.44 mmol) in a dropwise manner followed by the addition of a few drops of N,N-dimethylformamide (10 µL). The reaction mixture was stirred at ambient temperature for 16 h. The crude acyl chloride was then added to a stirred mixture of 3-amino-2-methylphenol (54 mg, 0.44 mmol), *N,N*-diisopropylethylamine (397 µL, 2.28 mmol) and

dichloromethane (1 mL) and stirred at ambient temperature for 2-16 h. The solvent was removed under reduced pressure. The crude product was taken up in saturated aq. $NaHCO_3$ (5 mL) and extracted with ethyl acetate (3 × 10 mL). The combined organic components were then washed with brine (10 mL), dried over $MgSO_4$, filtered and concentrated under reduced pressure. The crude was purified by column chromatography (silica 12 g, 0 to 40% ethyl acetate in petroleum ether) to yield the desired amide **3** as a white solid (13 mg, 10%).Rf 0.47 (petroleum ether:ethyl acetate 1:1); m.p. 238–240 °C; ^{1}H-NMR (500 MHz, DMSO-d6) δ 9.84 (s, 1H, CONH), 9.35 (s, 1H, OH), 8.10 (s, 1H, H-6), 8.07 (d, J 8.2, 2H, H-3), 8.03 (d, J 8.3, 2H, H-2), 7.00 (t, J 7.9, 1H, H-5'), 6.79 (d, J 7.8, 1H, H-6'), 6.73 (d, J 8.0, 1H, H-4'), 2.74 (s, 3H, 8-CH3), 2.03 (s, 3H, 2'-CH3); ^{13}C-NMR (126 MHz, DMSO-d6) δ 166.4 (CONH), 165.3 (C-8), 156.2 (C-5), 153.4 (C-3'), 137.9 (ArC), 137.3 (ArC), 134.1 (ArC), 128.7 (H-2), 126.2 (H-3), 126.0 (ArC), 121.3 (ArC), 118.0 (C-6'), 116.0 (C-6), 112.9 (C-4'), 19.4, (C-8) 11.4 (C-2'); IR (neat, v_{max}, cm^{-1}) 3291, 1640, 1607, 1499, 1466, 1307, 1174; LCMS (LCQ) Rt =2.5 min (method 1), m/z (ESI+) 325.1 $[M+H]^+$; HRMS (ESI): calcd. for $C_{18}H_{16}NaN_2OS$ $[M+Na]^+$ 347.0825, found 347.0827.

Methyl 4-methyl-3-((4-(2-methylthiazol-4-yl)benzoyl)amino)benzoate (4)

To 4-(2-methylthiazol-4-yl)benzoic acid (800 mg, 3.65 mmol) and methyl 3-amino-4-methylbenzoate (52 µL, 9.12 mmol) in tetrahydrofuran (15 mL) was added phosphorus trichloride (0.32 mL, 3.65 mmol). The reaction mixture was heated in a microwave reactor for 20 min at 150 °C. The crude product was taken up in saturated aq. $NaHCO_3$ (5 mL) and extracted with ethyl acetate (3 × 10 mL). The combined organic components were then washed with brine (10 mL), dried over $MgSO_4$, filtered and concentrated under reduced pressure. The crude was purified by column chromatography (amino silica 12 g, 0 to 50% ethyl acetate in petroleum ether) to yield the desired amide **4** as a white solid (920 mg, 65%). Rf 0.23 (petroleum ether:ethyl acetate 3:1); m.p. 179–181 °C; ^{1}H-NMR (500 MHz, DMSO-d6) δ 10.03 (s, 1H, CONH), 8.14 – 8.07 (m, 3H, H-3, H-6), 8.05 (d, J 8.3, 2H, H-2), 8.00 (d, J 1.8 , 1H, H-6'), 7.76 (dd, J 7.9, 1.8 , 1H, H-4'), 7.44 (d, J 7.9, 1H, H-9'), 3.85 (s, 3H, OCH3), 2.74 (s, 3H, 8-CH3), 2.33 (s, 3H, 2'-CH3); ^{13}C-NMR (126 MHz, DMSO-d6) δ 166.4 (CO), 165.6 (C-8), 153.3 (C-5), 140.0 (C-8'), 137.6 (C-1), 137.3 (C-7'), 133.7 (C-4), 131.3 (C-3'), 128.8 (C-2), 128.1 (C-6'), 127.5 (C-5'), 126.9 (C-4'), 126.3 (C-3), 116.1 (C-6), 52.5 (OCH3), 19.4 (8-CH3), 18.6 (2'-CH3). COO not visible; IR (neat, v_{max}, cm^{-1}) 3256, 1726, 1643, 1523, 1432, 1296, 1171, 1110; LCMS (LCQ) Rt = 2.6 min (method 1), m/z (ESI+) 367.0 $[M+H]^+$; HRMS m/z (ESI): calcd. for $C_{20}H_{18}N_2O_3S$ $[M+Na]^+$ 389.0930, found 389.0931.

4-Methyl-3-((4-(2-methylthiazol-4-yl)benzoyl)amino)benzamide (5)

Methyl 4-methyl-3-((4-(2-methylthiazol-4-yl)benzoyl)amino)benzoate

To 4-(2-methylthiazol-4-yl)benzoic acid (800 mg, 3.65 mmol) and methyl 3-amino-4-methylbenzoate (52 µL, 9.12 mmol) in tetrahydrofuran (15 mL) was added phosphorus trichloride (0.32 mL, 3.65 mmol). The reaction mixture was heated in a microwave reactor for 20 min at 150 °C. The crude product was taken up in saturated aq. $NaHCO_3$ (5 mL) and extracted with ethyl acetate (3 × 10 mL). The combined organic components were then washed with brine (10 mL), dried over $MgSO_4$, filtered and concentrated under reduced pressure. The crude was purified by column chromatography (amino silica 12 g, 0 to 50% ethyl acetate in petroleum ether) to yield the desired amide as a white solid (920 mg, 65%). Rf 0.23 (petroleum ether:ethyl acetate 3:1); m.p. 179–181 °C; ^{1}H-NMR (500 MHz, DMSO-d6) δ 10.03 (s, 1H, CONH), 8.14 – 8.07 (m, 3H, H-3, H-6), 8.05 (d, J 8.3, 2H, H-2), 8.00 (d, J 1.8 , 1H, H-6'), 7.76 (dd, J 7.9, 1.8 , 1H, H-4'), 7.44 (d, J 7.9, 1H, H-9'), 3.85 (s, 3H, OCH_3), 2.74 (s, 3H, 8-CH_3), 2.33 (s, 3H, 2'-CH3); ^{13}C-NMR (126 MHz, DMSO-d6) δ 166.4 (CO), 165.6 (C-8), 153.3 (C-5), 140.0 (C-8'), 137.6 (C-1), 137.3 (C-7'), 133.7 (C-4), 131.3 (C-3'), 128.8 (C-2), 128.1 (C-6'), 127.5 (C-5'), 126.9 (C-4'), 126.3 (C-3), 116.1 (C-6), 52.5 (OCH_3), 19.4 (8-CH_3), 18.6 (2'-CH_3). COO not visible; IR (neat, v_{max}, cm^{-1}) 3256, 1726, 1643, 1523, 1432, 1296, 1171, 1110; LCMS (LCQ) Rt = 2.6 min (method 1), m/z (ESI+) 367.0 $[M+H]^+$; HRMS m/z (ESI): calcd. for $C_{20}H_{18}N_2O_3S$ $[M+Na]^+$ 389.0930, found 389.0931.

4-Methyl-3-((4-(2-methylthiazol-4-yl)benzoyl)amino)benzoic acid

To methyl 4-methyl-3-((4-(2-methylthiazol-4-yl)benzoyl)amino)benzoate (920 mg, 2.51 mmol) in methanol (24 mL) was added 2 M aq. sodium hydroxide (12.6 mL, 25.1 mmol) and the mixture stirred at an ambient temperature for 16 h. The reaction mixture was then heated for 2 h at 50 °C. The solvent was removed under reduced pressure. The crude was taken up in water and the mixture was acidified to a pH of 2–3 with 2 M aq. hydrochloric acid solution. The resulting precipitate was collected by vacuum filtration and dried under reduced pressure to afford the desired acid as a white solid (926 mg, 99%). m.p. 254–256 °C; ^{1}H-NMR (500 MHz, DMSO-d6) δ 12.85 (s, 1H, COOH), 10.04 (s, 1H, CONH), 8.13 – 8.07 (m, 3H, H-3, H-6), 8.06 (d, J 8.3, 2H, H-2), 7.95 (d, J 1.7, 1H, H-6'), 7.74 (dd, J 7.9, 1.7, 1H, H-4'), 7.40 (d, J 7.9, 1H, H-3'), 2.74 (s, 3H, 8-CH_3), 2.32 (s, 3H, 2'-CH_3); ^{13}C-NMR (126 MHz, DMSO-d6) δ 167.4 (COOH), 166.4 (CONH), 165.6 (C-8), 153.3 (C-5), 139.5 (C-2'), 137.5 (C-1), 137.1 (C-1'), 133.8 (C-4), 131.1 (C-3'), 129.3 (C-5'), 128.7 (C-2), 127.8 (C-6'), 127.2 (C-4'), 126.3 (C-3), 116.01 (C-6), 19.4 (8-CH_3), 18.59 (2'-CH_3); IR (neat, v_{max}, cm^{-1}) 2923, 1679, 1638, 1512, 1492, 1414, 1390, 1251, 1178; LCMS (LCQ) Rt =3.0 min (method 1), m/z (ESI+) 353.0 $[M+H]^+$; HRMS (ESI): calcd. for $C_{19}H_{16}N_2NaO_3S$ $[M+Na]^+$ 375.0774, found 375.0774.

4-Methyl-3-((4-(2-methylthiazol-4-yl)benzoyl)amino)benzamide (5)

To 4- methyl-3-((4-(2-methylthiazol-4-yl)benzoyl)amino)benzoic acid (146) (100 mg, 0.28 mmol), EDCI (68 mg, 0.35 mmol), HOBt (54 mg, 0.35 mmol), *N,N*-diisopropylethylamine (100 µL, 0.57 mmol) in *N,N*-dimethylformamide (1 mL) was added 2 M ammonia in methanol (0.43 mL, 0.85 mmol). The reaction mixture was stirred at ambient temperature for 16 h. The solvent was removed under reduced pressure. The crude product was taken up in ethyl acetate (5 mL), washed with 1 M aq. hydrochloric acid solution. (4 mL), saturated aq. $NaHCO_3$ (4 mL), brine (4 mL), dried over $MgSO_4$, filtered and concentrated under reduced pressure. The crude was purified by column chromatography (amino silica 12 g, 0 to 5% methanol in dichloromethane) to yield the desired primary amide **5** as a white solid (39 mg, 37%)**.** Rf 0.17 (dichloromethane:methanol 19:1); m.p. 215–217 °C; ^{1}H-NMR (500 MHz, DMSO-d6) δ 10.02 (s, 1H, CONH), 8.14 – 8.08 (m, 3H, H-3. H-6), 8.05 (d, J 8.5, 2H, H-2), 7.91 (s, 1H, 5'-CONHAB), 7.86 (d, J 1.8, 1H, H-6'), 7.70 (dd, J 7.9, 1.8, 1H, H-4'), 7.35 (d, J 7.9, 1H, H-3'), 7.27 (s, 1H, 5'-CONHAB), 2.74 (s, 3H, 8-CH_3), 2.28 (s, 3H, 2'-CH_3); ^{13}C-NMR (126 MHz, DMSO-d6) δ 167.9 (CO), 166.4 (CO), 165.5 (C-8), 153.3 (C-5), 138.0 (C-2'), 137.5 (C-1), 136.8 (C-1'), 133.8 (C-4), 132.8 (C-5'), 130.6 (C-3'), 128.7 (C-2), 126.6 (C-6'), 126.3 (C-3), 125.6 (C-4), 116.0 (C-6), 19.4 (8-CH_3), 18.37 (2'-CH_3); IR (neat, ν_{max}, cm^{-1}) 3108, 1713, 1668, 1608, 1571, 1501, 1436, 1410, 1278; LCMS (LCQ) Rt =1.7 min (method 1), m/z (ESI+) 352.0 $[M+H]^+$; HRMS (ESI): calcd. for $C_{19}H_{17}N_3NaO_2S$ $[M+Na]^+$ 374.0934, found 374.0933.

4-Methyl-3-((4-(2-methyloxazol-4-yl)benzoyl)amino)benzamide (6)

Methyl 4-(2-methyloxazol-4-yl)benzoate

Methyl 4-(2-bromoacetyl)benzoate (400 mg, 1.56 mmol) was stirred in neat acetamide (276 mg, 4.67 mmol) at 160 °C for 2 h. Water was added to the reaction mixture. The resulting precipitate was collected by vacuum filtration and dried under reduced pressure to afford the desired compound 191 as a brown solid (308 mg, 87%) which was carried forward without further purification. ^{1}H-NMR (500 MHz, DMSO-d6) δ 8.07 (s, 1H, H-6), 8.00 (d, J 8.2, 2H, H-3), 7.89 (d, J 8.1, 2H, H-2), 3.86 (s, 3H, OCH_3), 2.48 (s, 3H, 8-CH_3).

4-(2-Methyloxazol-4-yl)benzoic acid

To methyl 4-(2-methyloxazol-4-yl)benzoate (191) (279 mg, 1.2 mmol) in methanol (5 mL) and water (1.5 mL) was added sodium hydroxide (150 mg, 3.86 mmol) and the reaction mixture stirred at ambient temperature for 16 h. Upon completion, the reaction mixture was acidified to pH of 2-3 using 2 M aq. hydrochloric acid solution. The resulting precipitate was collected by vacuum filtration and dried under reduced pressure to afford the desired acid as a as a white solid (130 mg, 47%). ^{1}H-NMR (500 MHz, DMSO-d6) δ 8.56 (s, 1H, 11, H-6), 7.97 (d, J 8.0, 2H, H-3), 7.85 (d, J 8.0, 2H, H-2), 2.47 (s, 3H, 8- CH_3); LCMS (LCQ) Rt = 0.5 min (method 1), m/z (ESI+) 204.2 [M+H]+ .

4-Methyl-3-((4-(2-methyloxazol-4-yl)benzoyl)amino)benzamide (6)

To 4-(2-methylthiazol-4-yl)benzoic acid (110 mg, 0.54 mmol) in dichloromethane (3 mL) was added oxalyl chloride (0.05 mL, 0.65 mmol) in a dropwise manner followed by *N,N*-dimethylformamide (10 µL). The reaction mixture was stirred at ambient temperature for 16 h. The crude acyl chloride was then added to a stirred mixture of 3-amino-4-methylbenzamide (98 mg, 0.65 mmol) followed by the addition of *N,N*-diisopropylethylamine (0.47 mL, 2.71 mmol). The reaction mixture was stirred at ambient temperature for 2-16 h. The solvent was removed under reduced pressure. The crude product was taken up in saturated aq. $NaHCO_3$ (5 mL) and extracted with ethyl acetate (3 × 10 mL). The combined organic components were then washed with brine (10 mL), dried over $MgSO_4$, filtered and concentrated under reduced pressure. The crude was purified by column chromatography (silica 12 g, 0 to 5% methanol in dichloromethane) to yield the desired amide **6** as a white solid (55 mg, 29%). Rf 0.28 (dichloromethane:methanol 19:1); m.p. 260–262 °C; ^{1}H-NMR (500 MHz, DMSO-d6) δ 10.00 (s, 1H, CONH), 8.61 (s, 1H, H-6), 8.05 (d, J 8.1, 2H, H-3), 7.91 (d, J 8.4, 3H, H-2, 5'-CONHAB), 7.86 (s, 1H, H-6'), 7.70 (dd, J 7.9, 1.9, 1H, H-4'), 7.35 (d, J 7.9, 1H, H-3'), 7.27 (s, 1H, 5'-CONHAB) 2.28 (s, 3H, 2'-CH_3). 8-CH_3 under DMSO peak; ^{13}C-NMR (126 MHz, DMSO-d6) δ 167.8 (CO), 165.4 (CO), 162.2 (C-8), 139.4 (C-5), 137.9 (C-2'), 136.8 (ArC), 136.3 (ArC), 134.6 (C-1), 133.8 (C-4), 132.8 (C-5'), 130.6 (C-3'), 128.7 (C-2), 126.6 (C-6'), 125.5 (C-4'), 125.33 (C-3), 18.4 (8-CH_3), 14.0 (2'-CH_3); IR (neat, , v_{max}, cm^{-1}) 3255, 1673, 1635, 1616, 1522, 1489, 1386, 1276, 1214; LCMS (LCQ) Rt =0.8 min (method 1), m/z (ESI+) 336.1 $[M+H]^+$; HRMS (ESI): calcd. for $C_{19}H_{17}N_3NaO_3$ $[M+Na]^+$ 358.1162, found 358.1150.

_N_-(6-methyl-2-pyridyl)-4-(2-methylthiazol-4-yl)benzamide (7)

To 4-(2-methylthiazol-4-yl)benzoic acid (80 mg, 0.36 mmol) in dichloromethane (3 mL) was added oxalyl chloride (37 µL, 0.44 mmol) in a dropwise manner followed by *N,N*-dimethylformamide (10 µL). The reaction mixture was stirred at ambient temperature for 16 h. The crude acyl chloride was then added to a stirred mixture of 2-amino-6-methylpyridine (40 mg, 0.36 mmol) followed by the addition of *N,N*-diisopropylethylamine (397 µL, 2.28 mmol). The reaction mixture was stirred at ambient temperature for 2-16 h. The solvent was removed under reduced pressure. The crude product was taken up in saturated aq. $NaHCO_3$ (5 mL) and extracted with ethyl acetate (3 × 10 mL). The combined organic components were then washed with brine (10 mL), dried over $MgSO_4$, filtered and concentrated under reduced pressure. The crude was purified by column chromatography (silica 12 g, 0 to 45% ethyl acetate in petroleum ether) to yield the desired amide **7** as a colourless solid (54 mg, 45%). Rf 0.48 (petroleum ether:ethyl acetate 1:1); m.p. 195–197 °C; ^{1}H-NMR (500 MHz, DMSO-d6) 10.69 (s, 1H), 8.13 (s, 1H), 8.10 (d, J 8.2, 2H), 8.06 (d, J 8.0, 2H), 8.02 (d, J 8.2, 1H), 7.73 (t, J 7.8, 1H), 7.03 (d, J 7.3, 1H), 2.74 (s, 3H), 2.46 (s, 3H); ^{13}C-NMR (126 MHz, DMSO-d6) 166.4, 165.9, 157.0, 153.3, 152.0, 138.8, 137.6, 133.5, 129.1, 126.1, 119.5, 116.2, 112.1, 24.0, 19.4;

IR (neat, v_{max}, cm^{-1}) 3314, 2923, 1610, 1539, 1522, 1290, 1169; LCMS (LCQ) Rt = 3.1 min (method 1), m/z (ESI+) 310.1 $[M+H]^+$; HRMS (ESI): calcd. for $C_{17}H_{16}N_3OS$ $[M+H]^+$ 310.1009, found 310.1012.

1-(4-Fluoro-3-(trifluoromethyl)phenyl)-3-(5-(4-pyridyl)-1,3,4-thiadiazol-2-yl)urea (ML216)[44]

Phenyl-5-(4-pyridyl)-1,3,4-thiadiazol-2-ylcarbamate

Sodium hydride (700 mg, 33.7 mmol) was slowly added to a suspension of 5-(4-pyridyl)-1,3,4-thiadiazol-2-yl-amine (2.00 g, 11.2 mmol) in tetrahydrofuran (40 mL) at 0 °C. The resulting reaction mixture was stirred at 0 °C for 2 h. Diphenyl carbonate (2.89 g, 13.5 mmol) was added and the reaction mixture was stirred at 0 °C for 30 min. The reaction mixture was warmed to ambient temperature and stirred overnight. Dichloromethane (40 mL) and brine (10 mL) was added to the reaction mixture and the solid precipitate was collected by filtration to yield the desired compound as a crystalline off-white solid (3.10 g, 93%). Rf 0.52 (dichloromethane:methanol 19:1); m.p. 278–280 °C; ^{1}H-NMR (500 MHz, DMSO-d6) δ 8.58 (d, J 4.9, 2H, H-2), 7.70 (d, J 4.9, 2H, H-3), 7.33 (t, J 7.6, 2H, H-15), 7.11 (t, J 7.4, 1H, H-17), 7.07 (d, J 7.7, 2H, H-16); ^{13}C-NMR (126 MHz DMSO-d6) δ = 174.7 (CO), 162.1 (ArC), 155.1 (ArC), 153.7 (C-14), 150.7 (C-2), 140.1 (ArC), 129.2 (C-15), 124.0 (C-17), 122.4 (C-16), 120.2 (C-3); IR (neat, v_{max}, cm^{-1}) 3542, 3118, 2417, 1604, 1460, 1319, 1296, 1208, 1113; LCMS (LCQ) Rt = 1.8 min (method 2), m/z (ESI+) 299.03 $[M+H]^+$; HRMS (ESI): calcd. for $C_{14}H_{11}N_4O_2S$ $[M+H]^+$ 299.0598, found 299.0597.

*1-(4-Fluoro-3-(trifluoromethyl)phenyl)-3-(5-(4-pyridyl)-1,3,4-thiadiazol-2-yl)urea (**ML216**)*

To a suspension of phenyl -(5-(4-pyridyl)-1,3,4-thiadiazol-2-yl)carbamate (150 mg, 0.50 mmol) in toluene (5 mL) was added 4-fluoro-3-(trifluoromethyl)aniline (65 µL, 0.50 mmol). The reaction mixture was heated in a microwave reactor at 150 °C for 30 min and the resulting suspension was cooled to room temperature. The reaction mixture was concentrated under reduced pressure. The resulting solid 223 was triturated with dichloromethane (5 mL) and further triturated with 5% methanol in dichloromethane (3 mL) to yield the desired compound **ML216** as an orange solid (82 mg, 46%). ^{1}H-NMR (500 MHz, DMSO-d6) δ 11.61 (s, 1H, NH-urea), 9.52 (s, 1H, NH-urea), 8.73 (d, *J* 5.9, 2H, H-2), 8.06 (s, 1H, H15), 7.89 (d, *J* 5.3, 2H, H-3), 7.77 (s, 1H, H-19), 7.49 (t, *J* 9.7, 1H, H-18); LCMS (LCQ) Rt = 2.7 min (method 1), m/z (ESI+) 384.0 [M+H]+ . ^{1}H-NMR consistent with literature data[44].

SUPPLEMENTARY TABLE 1. Statistics for data collection, phasing and refinement

	BLM-HD$^{\Delta WHD}$ + ADP	Liganded-BLM-HD$^{\Delta WHD}$
Data collection		
Space group	$P2_1$	P1
Cell dimensions		
a, b, c (Å)	54.28, 107.69, 55.20	84.69, 111.60, 132.38
α, β, γ (º)	90.00, 109.31, 90.00	72.70, 80.13, 79.24
Wavelength	0.9780	0.9762
Resolution (Å)	51.23 – 1.53 (1.56– 1.53)	125.37 – 2.97 (3.08 – 2.97)
Mn I / σI	12.7 (1.2)	7.8 (1.4)
Mn I, $CC_{1/2}$	1.00 (0.61)	0.99 (0.57)
Completeness (%)	98.3 (90.3)	98.0 (94.5)
Redundancy	1.9 (1.7)	2.6 (2.7)
Refinement		
Resolution (Å)	51.23 – 1.53 (1.56– 1.53)	47.28-2.97 (3.07-2.96)
No. unique reflections	88464 (8096)	91661 (8892)
R_{work} / R_{free}	0.19 / 0.21	0.23 / 0.27
No. atoms		
Macromolecules	3870	24954
Ligands	65	427
Solvent	438	91
B-factors		
Wilson	32.58	77.77
ADP (mean)		
Macromolecules	31.00	95.79
Ligands	40.89	98.56
Solvent	45.69	53.65
R.m.s. deviations		
Bond lengths (Å)	0.014	0.006
Bond angles (º)	1.64	1.11
Molprobity		
All atom clashscore	2.44	7.42
Ramachandran		
Outliers	0.21 %	0.42 %
Allowed	1.65 %	3.72 %
Favoured	98.15 %	95.85 %

* values in parentheses are for the highest resolution shell

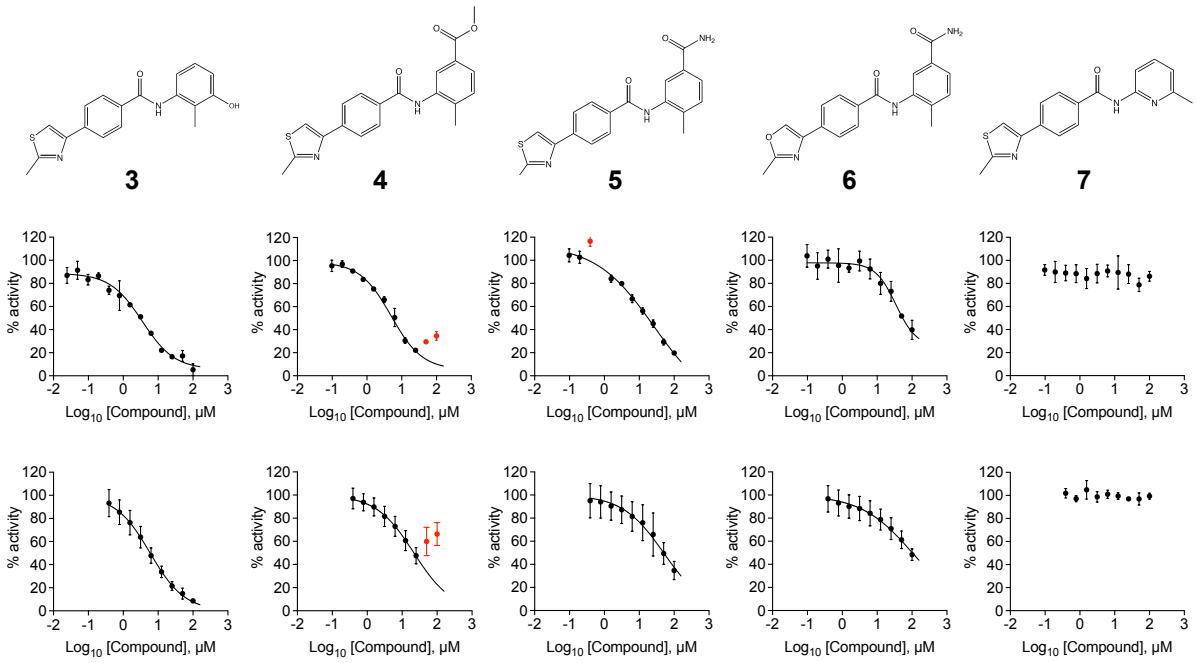

Figure S1

(Top) Chemical drawings for compounds **3** to **7.** (Middle) Dose response curves from fluorescence-based DNA unwinding assays with BLM-HD. Data points are the mean of three technical replicates with error bars representing 1 SD. **(**Bottom) Dose response curves from ATP turnover assays with BLM-HD. Data points represent the mean from at least two individual experiments, each containing 3 technical replicates. Error bars represent the standard error of the mean (SEM). Experimental data were fitted with a four parameter, log(inhibitor) vs. response model with variable slope. Calculated values for IC_{50}, Hill slope (*n*H) and 95% confidence intervals (95% CI) are reported in Table 1. Data points excluded from fitting are coloured red.

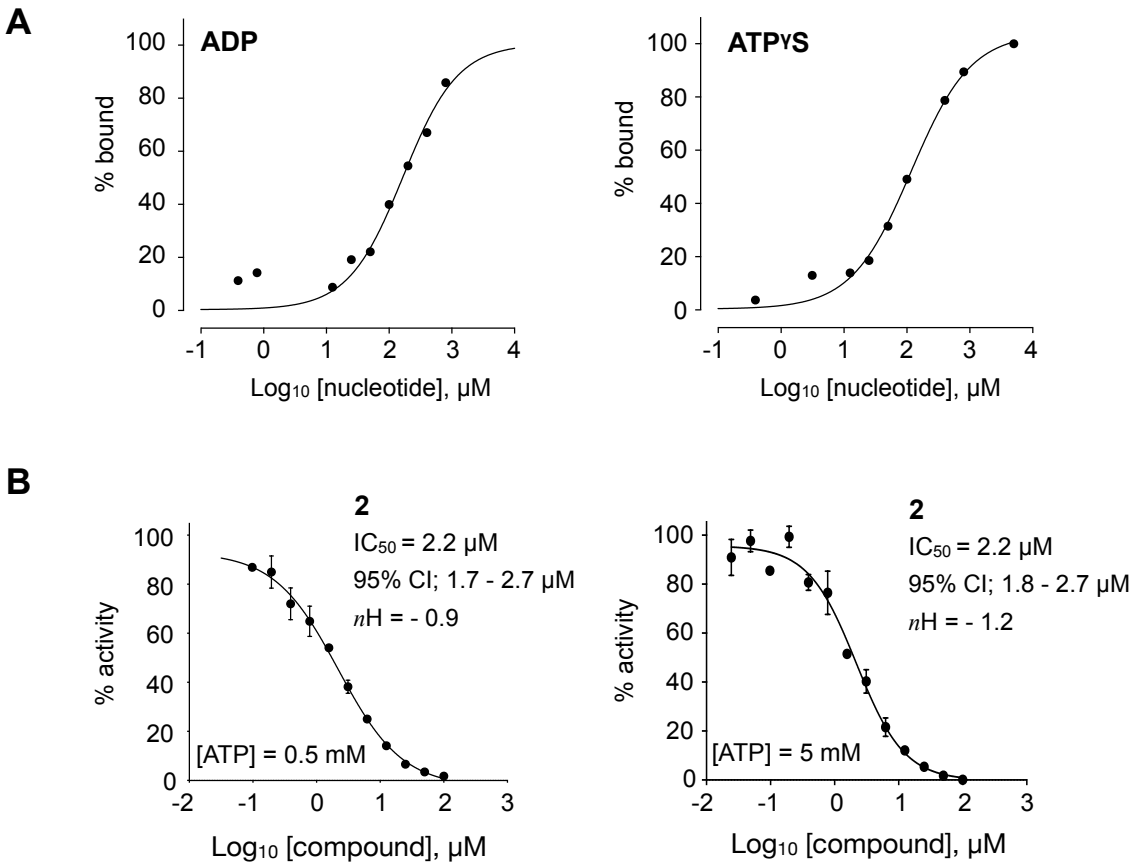

Figure S2

(A) Indicative binding isotherms for titrations of Mg-ADP and Mg-ATPγS into BLM-HD as measured by MST. Fitted lines are intended as visual aids only, as the data only represent values from a single preliminary experiment. (B) Dose response curves from fluorescence-based DNA unwinding assays with BLM-HD, carried out at two different ATP concentrations. Experimental data were fitted with a four parameter, log(inhibitor) vs. response model with variable slope. Calculated values for IC_{50}, Hill slope (*n*H) and 95% confidence intervals (95% CI) are given in each case. Data points represent the mean of 3 technical replicates, with error bars representing 1 SD.

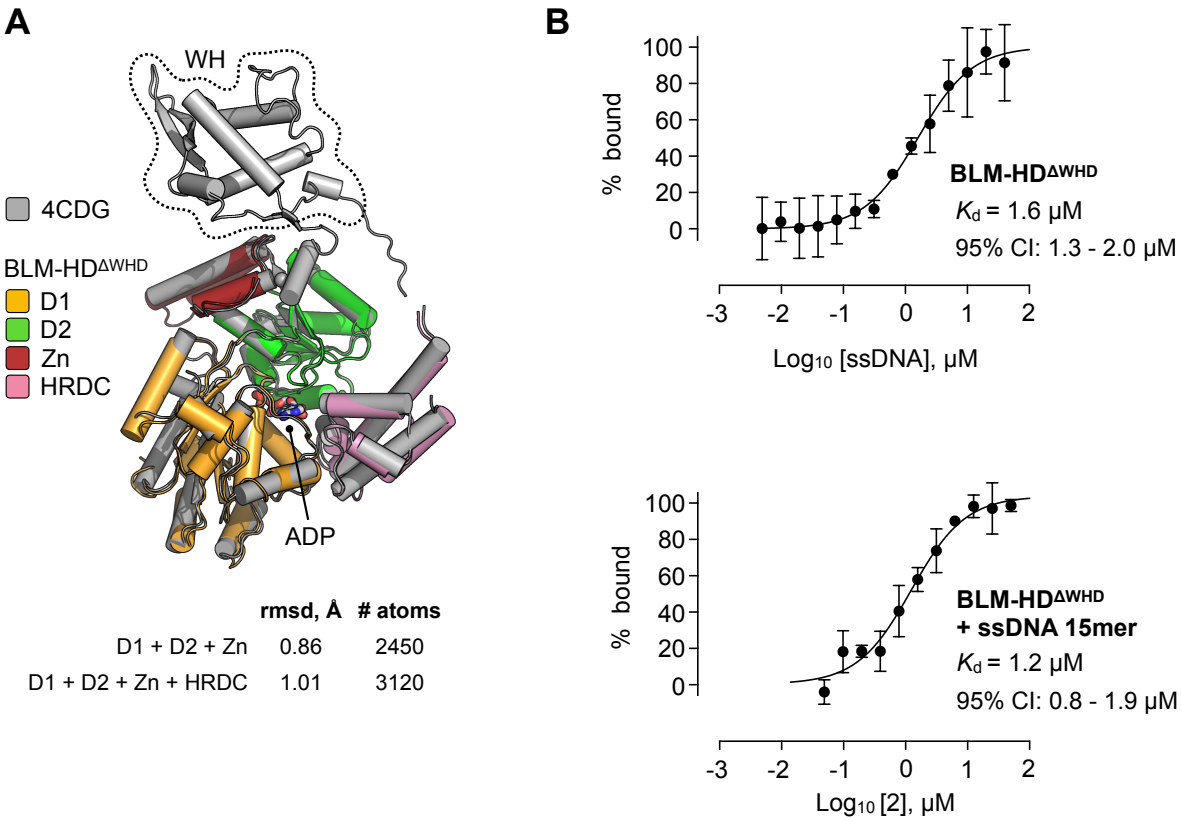

Figure S3

(A) Superposition of the structures of BLM-HD (PDB: 4CDG) and BLM-HD$^{\Delta WHD}$ using PyMOL [45]. Values for rmsd in Angstrom are shown, calculated over the indicated number of equivalent atoms. See associated key for details of colour scheme. (B) Isotherms for binding of BLM-HD$^{\Delta WHD}$ to (top) ssDNA-15mer and (bottom) compound **2** in the presence of ssDNA-15mer, as determined by MST. Values for K_d and 95% CI are given in each case. For all plots, data represent the mean of three technical replicates with error bars representing 1 SD.

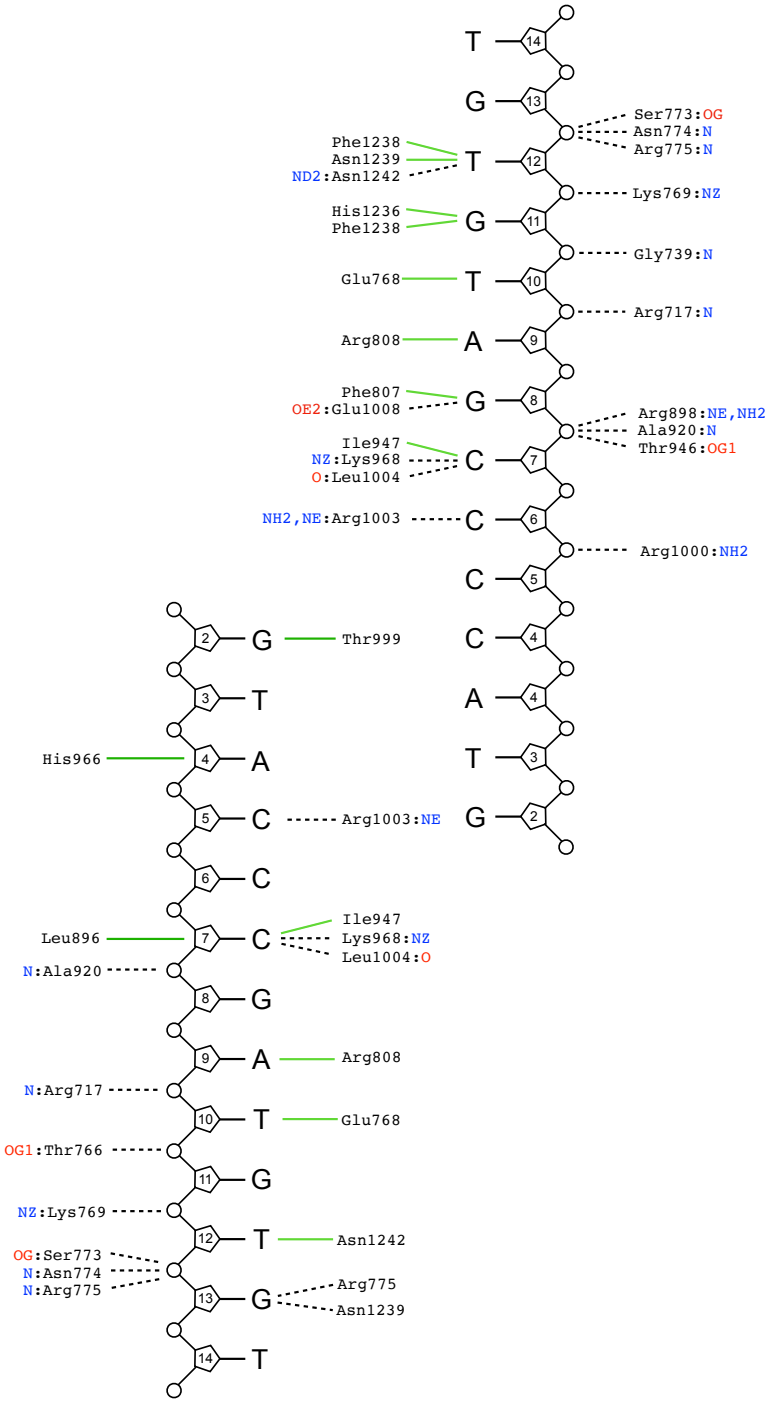

Figure S4

Schematic summary of DNA-interactions made within the crystal lattice of the liganded complex (BLM-HD$^{\Delta WHD}$ + Mg-ADP + ssDNA-15mer + compound **2**). Interaction network determined through by the PDBsum Generate webserver[46]. Green solid lines represent hydrophobic / stacking interactions. Black dotted lines represent potential hydrogen bonds.

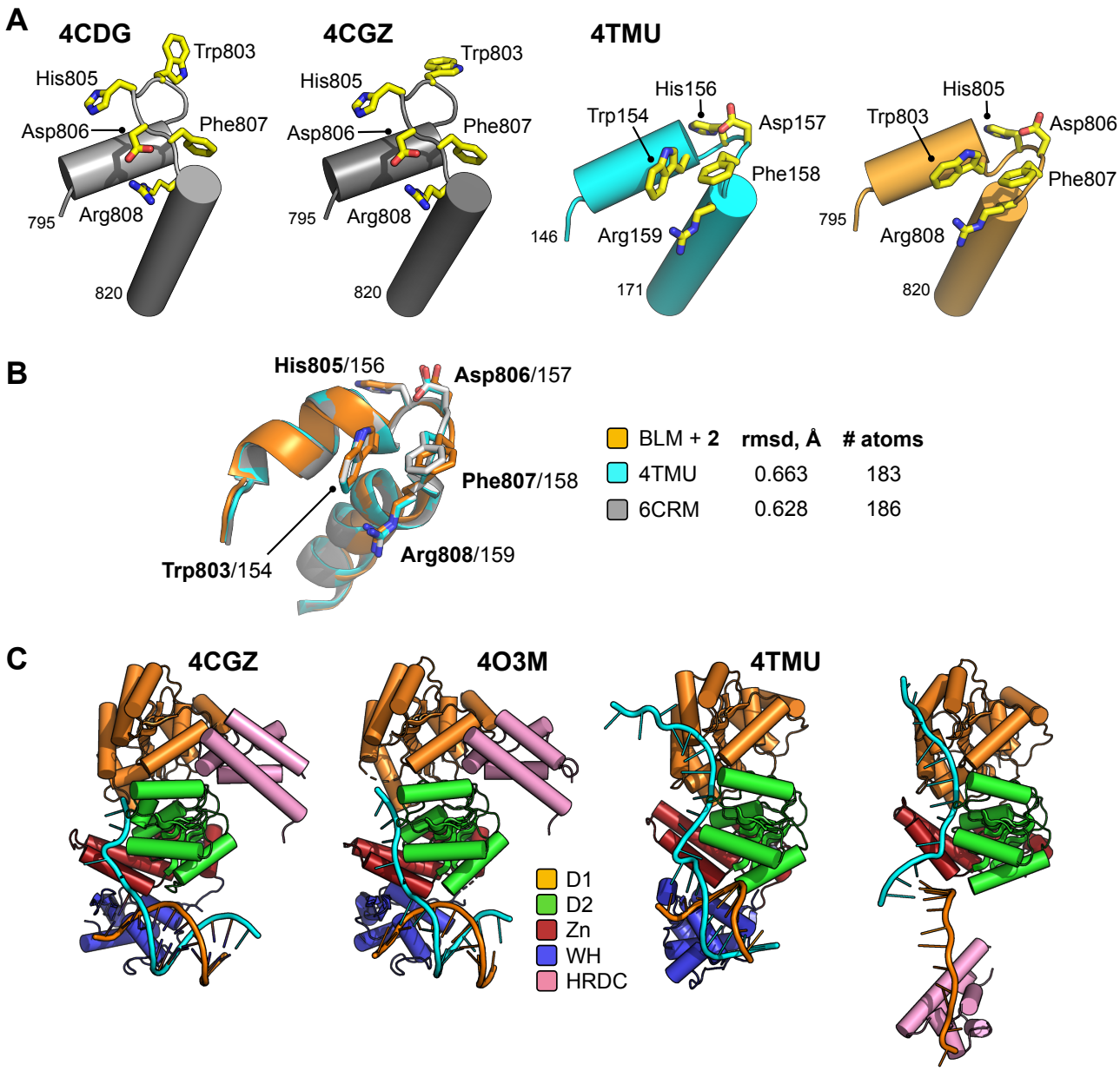

Figure S5

(A) Molecular secondary structure cartoons showing selected amino acid side chains of the aromatic rich loop (ARL) region in PDB entries 4CDG and 4CGZ (BLM-HD) and 4TMU (Cronobacter sakazakii RecQ) to that reported here for liganded-BLM-HDΔWHD. Amino acid numbering is provided for the start and end of the region compared, with the identity of key residues also provided. (B) Superposition of the ARL in liganded-BLM-HDΔWHD (coloured orange) with those found in PDB entries 4TMU (cyan) and 6CR[23] (grey); which both represent structures of the catalytic core of C. sakazakii RecQ in complex with different DNA substrates. (C) Molecular cartoon representations of the helicase catalytic cores reported in PDB entries 4CGZ, 4O3M and 4TMU, highlighting their respective interactions with bound DNA substrates and comparing this to liganded-BLM-HD$^{\Delta WHD}$. Additional details for the colour scheme can be found in the associated key.